Bifurcations in nonlinear dynamical systems

Consider the nonlinear dynamical system

$$\frac{d\boldsymbol{x}}{dt} = \boldsymbol{f}(\boldsymbol{x}, \mu) \tag{1}$$

where μ is a real parameter which we are allowed to vary[1]. In this course note we study bifurcations of the flow generated by (1) as we vary the parameters. Such bifurcations can be defined as topological changes in the flow map and they can be grouped into two broad classes

- **Local bifurcations**: these bifurcations involve a small portion of the phase space. Examples of local bifurcations are bifurcation of equilibria, e.g., zero-eigenvalue bifurcations (saddle-node, transcritical, subcritical/supercritical pitchfork), Hopf bifurcations, Bogdanov-Takens bifurcation, etc.
- **Non-local bifurcations**: these bifurcations usually involve large portions of the phase space. Examples of non-local/global bifurcations are homoclinic and heteroclinic bifurcations (see Figure 1), saddle-node bifurcation of cycles, etc. Non-local bifurcations are usually associated with significant changes in the phase portrait.

Bifurcations are related to the notion of *structural stability* of a dynamical system. Roughly speaking, if the qualitative behavior of the system remains the same for all vector fields nearby a particular $\boldsymbol{f}(\boldsymbol{x}, \mu)$ then the system (1) (or the vector field $\boldsymbol{f}(\boldsymbol{x}, \mu)$) is said to be *structurally stable*. Mathematically we can define structural stability as follows.

Definition 1 (Structural stability)**.** A continuously differentiable vector field $\boldsymbol{f}$ is said to be structurally stable if there exists $\epsilon > 0$ such that *for all* continuously differentiable $\boldsymbol{g}$ that are "close enough" to $\boldsymbol{f}$, i.e.,

$$\|\boldsymbol{f} - \boldsymbol{g}\| < \epsilon \tag{2}$$

we have that f and g are *topologically equivalent*, i.e., there exists a homeomorphism whih maps trajectories of $\dot{\boldsymbol{x}} = \boldsymbol{f}(\boldsymbol{x})$ onto trajectories of $\dot{\boldsymbol{x}} = \boldsymbol{g}(\boldsymbol{x})$ and preserves their orientation by time.

Note that this definition relies on finely detailed information about the structure of flows generated by nonlinear dynamical systems, which is often very hard to obtain, especially in high dimensions. However, in two-dimensions things are way more manageable due to topological constraints on 2D flows such the Poincaré-Bendixson theorem. As a matter of fact, in 1962 Maurício Peixoto proved the following Theorem, which completely characterizes structural stability in 2D systems.

Theorem 1 (Peixoto - Structural stability for planar systems)**.** Let $\boldsymbol{f}(\boldsymbol{x}, \mu)$ be a continuously differentiable field on a compact subset U of the phase plane. Then $\boldsymbol{f}$ is structurally stable if and only if: (i) the number of fixed points and cycles U is finite and each is hyperbolic[2]; (ii) there are no trajectories connecting saddle points (see Figure 1 for a counterexample); iii) the nonwandering set in U[3] consists of periodic orbit and fixed points alone.

According to this theorem, planar systems with non-hyperbolic fixed points are *not* structurally stable. Unfortunately, no generalization of Peixoto's theorem is available in higher dimensions (even in three dimensions). The reason is that the definition of structural stability (Definition (1)) relies on finely detailed

[1] More generally, the dynamical system (1) can depend on multiple parameters

$$\boldsymbol{\mu} = (\mu_1, \ldots, \mu_M).$$

[2] It is possible to have bifurcation of periodic orbits, e.g., saddle-node bifurcation of cycles.

[3] A point $\boldsymbol{x} \in U$ is called "nonwandering" if, for *any* neighborhood B of $\boldsymbol{x}$, there exists T such that $\boldsymbol{X}(t, B) \cap B \neq \emptyset$ for all $t > T$. The nonwandering set consists of all nonwandering points.

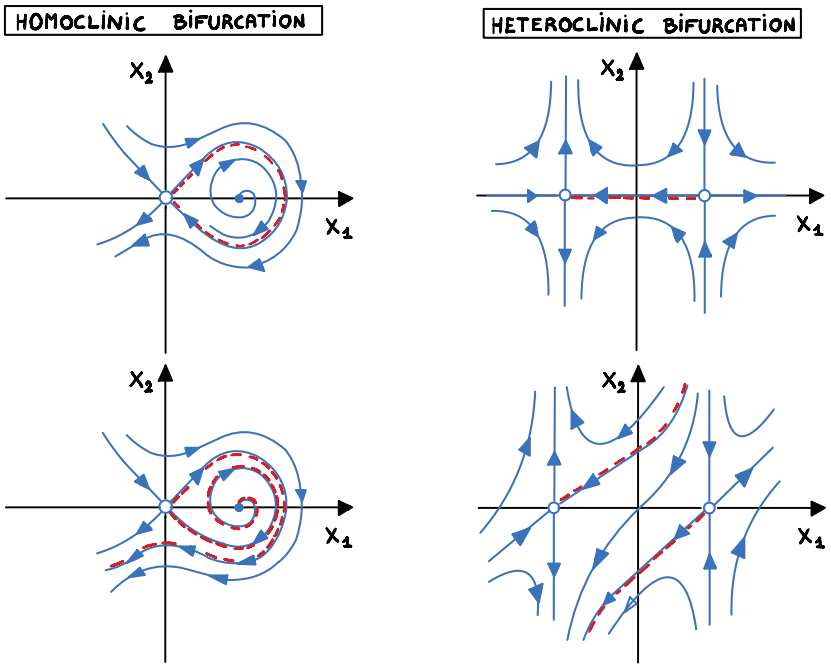

Figure 1: Examples of homoclinic and heteroclinic bifurcations in two-dimensional dynamical systems. An example of a two-dimensional system that yields the heteroclinic bifurcation shown above is $\dot{x}_1 = x_1^2 - 1$, $\dot{x}_2 = -x_2 x_1 + \mu(x_1^2 - 1)$.

information about the structure of flow and its perturbations, which is not generally available. This is one of the reason why attempts to construct a systematic bifurcation theory for general nonlinear dynamical systems led to very difficult technical questions. Of course, we can just focus our analysis on specific types bifurcations of dynamical systems, e.g., local bifurcations of equilibria. In this case, there is a rather systematic theory that allows us to come up with quantitative results.

Local bifurcations of equilibria. As is well known, the fixed points (equilibria) of the system (1) are solution of the algebraic equation

$$\boldsymbol{f}(\boldsymbol{x}, \mu) = \boldsymbol{0}. \tag{3}$$

By using the implicit function theorem, it is immediate to conclude that as the parameter μ varies, the fixed points $\boldsymbol{x}^*(\mu)$ are described by smooth functions of μ, except at points $(\boldsymbol{x}^*, \mu^*)$ where the Jacobian $\boldsymbol{J}_{\boldsymbol{f}}(\boldsymbol{x}, \mu)$ is not invertible, i.e., it has at least one zero eigenvalue.

Theorem 2 (Implicit function theorem)**.** Let $\boldsymbol{f}(\boldsymbol{x}, \mu)$ be continuously differentiable in a neighborhood of a fixed point $(\boldsymbol{x}^*, \mu^*)$, i.e., a point such that $\boldsymbol{f}(\boldsymbol{x}^*, \mu^*) = \boldsymbol{0}$. If the Jacobian matrix

$$\boldsymbol{J}_{\boldsymbol{f}}(\boldsymbol{x}^*, \mu^*) = \begin{bmatrix} \dfrac{\partial f_1(\boldsymbol{x}^*, \mu^*)}{\partial x_1} & \cdots & \dfrac{\partial f_1(\boldsymbol{x}^*, \mu^*)}{\partial x_n} \\ \vdots & \ddots & \vdots \\ \dfrac{\partial f_n(\boldsymbol{x}^*, \mu^*)}{\partial x_1} & \cdots & \dfrac{\partial f_n(\boldsymbol{x}^*, \mu^*)}{\partial x_n} \end{bmatrix} \tag{4}$$

is nonsingular (invertible) then there exists a neighborhood B of μ^* (i.e., an interval that includes μ^*) in which the zero level set of $\boldsymbol{f}(\boldsymbol{x}, \mu)$ can be represented as a graph of a smooth function $\boldsymbol{x}^*(\mu)$, i.e.,

$$\boldsymbol{f}(\boldsymbol{x}^*(\mu), \mu) = \boldsymbol{0} \qquad \text{for all } \mu \in B. \tag{5}$$

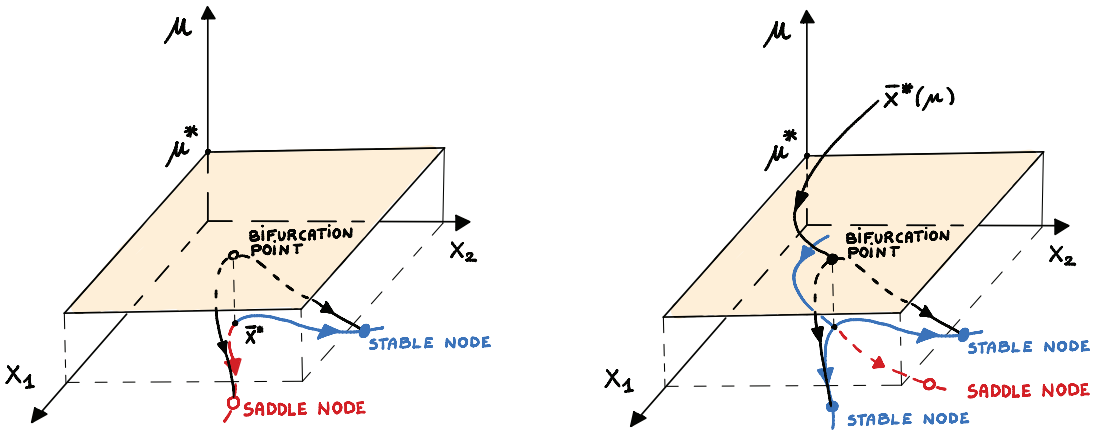

Figure 2: Bifurcation diagrams corresponding to a saddle-node bifurcation and a supercritical pitchfork bifurcation in a two-dimensional dynamical system. The stability properties of each of the fixed points can change as μ is varied. For instance, a stable node can turn into a stable spiral as μ is varied.

The function $\boldsymbol{x}^*(\mu)$ is continuously differentiable with respect to μ in B, and it interpolates $(\boldsymbol{x}^*, \mu^*)$. Moreover[4],

$$\frac{d\boldsymbol{x}^*(\mu^*)}{d\mu} = -\boldsymbol{J}_{\boldsymbol{f}}^{-1}(\boldsymbol{x}^*, \mu^*)\frac{\partial \boldsymbol{f}(\boldsymbol{x}^*, \mu^*)}{\partial \mu}. \tag{8}$$

Broadly speaking, the implicit function theorem asserts that if $\boldsymbol{J}_{\boldsymbol{f}}(\boldsymbol{x}^*, \mu^*)$ is invertible (no-zero eigenvalues) then the graph of each function $\boldsymbol{x}^*(\mu)$ is a smooth branch of equilibria of (1) (see Figure 2). On the other, hand if $\boldsymbol{J}_{\boldsymbol{f}}(\boldsymbol{x}^*, \mu^*)$ is not invertible at some point $(\boldsymbol{x}^*, \mu^*)$ then several branches of equilibria may (or may not) intersect there. In this case, $(\boldsymbol{x}^*, \mu^*)$ is potential bifurcation point.

In Figure 2 we sketch the bifurcation diagrams corresponding to two rather common bifurcations, i.e., a saddle-node bifurcation and a pitchfork bifurcation in two dimensions. Both these bifurcations are called *zero eigenvalue bifurcations*, because they are characterized by a single real eigenvalue of the Jacobian matrix crossing the imaginary axis as the parameter μ is varied.

Hereafter we study two types of local bifurcations of equilibria depending on one real parameter μ:

1) **Zero-eigenvalue bifurcations**: These bifurcations are characterized by a single real eigenvalue crossing the imaginary axis as μ is varied (see Figure 3). Examples of zero-eigenvalue bifurcations:
   - Saddle-node bifurcation,
   - Transcritical bifurcation,
   - Supercritical/Subcritical pitchfork bifurcation,
   - $(\dots)$.

[4]Property (8) follows by differentiating (5) with respect to μ and evaluating the derivative at at $\mu = \mu^*$. In fact,

$$\boldsymbol{f}(\boldsymbol{x}^*(\mu), \mu) = \boldsymbol{0} \quad \Rightarrow \quad \frac{d\boldsymbol{f}(\boldsymbol{x}^*(\mu), \mu)}{d\mu} = \frac{\partial \boldsymbol{f}(\boldsymbol{x}^*(\mu), \mu)}{\partial \mu} + \sum_{j=1}^{n} \frac{\partial \boldsymbol{f}(\boldsymbol{x}^*(\mu), \mu)}{\partial x_j}\frac{dx_j^*(\mu)}{d\mu} = \boldsymbol{0}. \tag{6}$$

This equation can be written as

$$\boldsymbol{J}_{\boldsymbol{f}}(\boldsymbol{x}^*(\mu), \mu)\frac{d\boldsymbol{x}^*(\mu)}{d\mu} = -\frac{\partial \boldsymbol{f}(\boldsymbol{x}^*(\mu), \mu)}{\partial \mu}. \tag{7}$$

Recalling that $\boldsymbol{x}^*(\mu^*) = \boldsymbol{x}^*$ and evaluating (7) at $\mu = \mu^*$ yields (8).

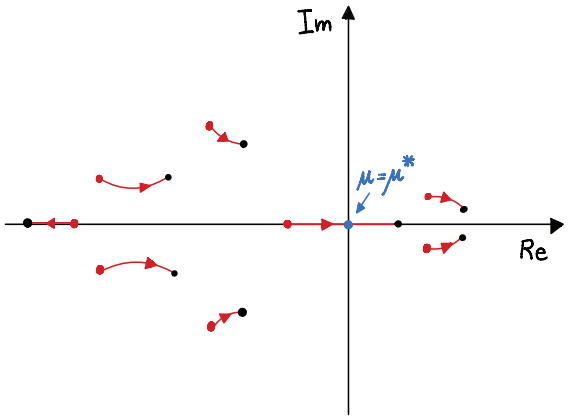

Figure 3: Zero eigenvalue bifurcations are characterized by a single real eigenvalue crossing the imaginary axis as the parameter μ is varied. Shown is a sketch of the eigenvalues $\lambda_j(\mu)$ of the Jacobain matrix $J_{\boldsymbol{f}}(\boldsymbol{x}^*(\mu),\mu)$ evaluated at the fixed point $\boldsymbol{x}^*(\mu)$. As μ is varied the eigenvalues move from the red dots to the black dots. At $\mu=\mu^*$ one real eigenvalue crosses the imaginary axis.

2) **Hopf bifurcations**: These bifurcations are characterized by a pair of complex conjugate eigenvalues crossing the imaginary axis as μ is varied (see Figure 8). There are two main kinds of Hopf bifurcations:

   - Supercritical Hopf bifurcation,
   - Subcritical Hopf bifurcation.

To study bifurcations of equilibria it is convenient to write the parametric dependence in (1) in terms of an additional ODE as

$$\begin{cases} \dfrac{d\boldsymbol{x}}{dt} = \boldsymbol{f}(\boldsymbol{x},\mu) \\ \dfrac{d\mu}{dt} = 0 \end{cases} \tag{9}$$

This is called *extended system*. By using the *normal form theorem* and the *local center manifold theorem* (see the course note 5) applied to the extended system (9), it is possible two write the local behavior of the system at any bifurcation point. The normal form of the system at the bifurcation point depends on the particular bifurcation.

Zero-eigenvalue bifurcations. Zero eigenvalue bifurcations are characterized by a single real eigenvalue $\lambda_i(\mu)$ of the Jacobian matrix $\boldsymbol{J_f}(\boldsymbol{x}^*(\mu),\mu)$ crossing the imaginary axis with non-zero "velocity" $d\lambda_i/d\mu$ as the parameter μ is varied (see Figure 3). Let us begin our analysis of zero-eigenvalue bifurcations by considering two-dimensional systems of the form

$$\begin{cases} \dot{x}_1 = f_1(x_1,x_2,\mu) \\ \dot{x}_2 = f_2(x_1,x_2,\mu) \end{cases} \tag{10}$$

In this case, zero-eigenvalue bifurcations have a clear geometric interpretation.

Theorem 3 (Zero-eigenvalue bifurcations in two-dimensional systems)**.** Zero-eigenvalue bifurcations in two-dimensional systems of the form (10) occur at points where the nullclines of the system are either *tangent* to each other, or at points[5] where one of the gradients ∇f_1 or ∇f_2 is zero.

[5]Note that the gradient of $f_i(x_1,x_2)$ is zero at points in which the zero level set of f_i intersect itself, e.g., the point

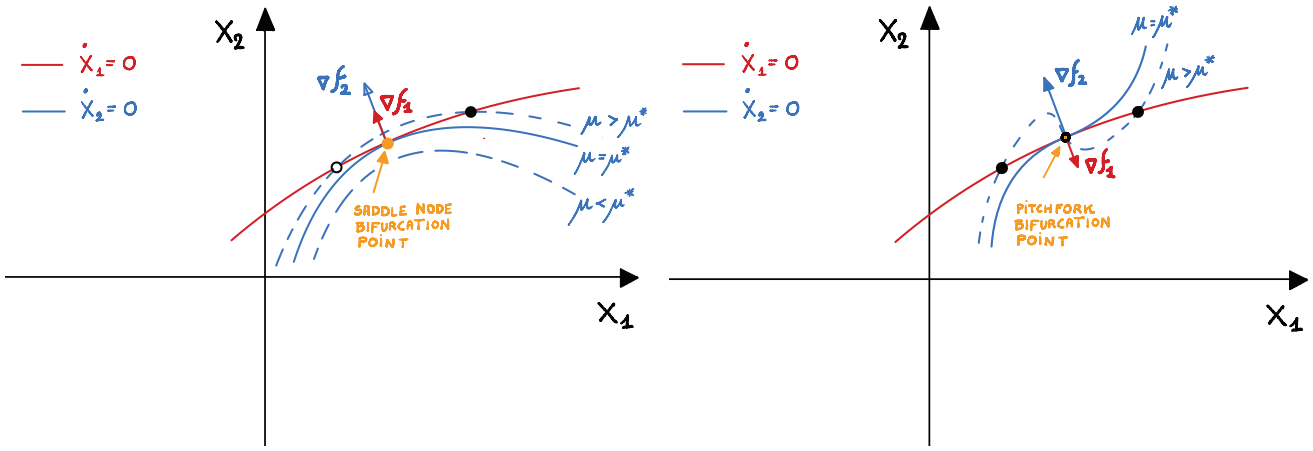

Figure 4: Graphical illustration of Theorem 3 for saddle-node and pitchfork bifurcations. The bifurcations occurs at locations where the nullclines are tangent. This makes the Jacobian matrix of the the vector field not invertible, i.e., the Jacobian has one zero eigenvalue.

Proof. Let us recall that the nullclines of a two-dimensional system are defined to be the zero level sets of $f_1(x_1, x_2, \mu)$ and $f_1(x_1, x_2, \mu)$, i.e.,

$$f_1(x_1, x_2, \mu) = 0 \quad (\dot{x}_1 = 0 \text{ nullcline}), \qquad f_2(x_1, x_2, \mu) = 0 \quad (\dot{x}_2 = 0 \text{ nullcline}). \tag{11}$$

We also know that the gradients

$$\nabla f_1 = \left(\frac{\partial f_1}{\partial x_1}, \frac{\partial f_1}{\partial x_2} \right), \qquad \nabla f_2 = \left(\frac{\partial f_2}{\partial x_1}, \frac{\partial f_2}{\partial x_2} \right) \tag{12}$$

are orthogonal to each level set of f_1 and f_2, respectively. In particular, they are orthogonal to the zero level sets of f_1 and f_2. The Jacobian matrix of (10) can be written as

$$\boldsymbol{J_f} = \begin{bmatrix} \dfrac{\partial f_1}{\partial x_1} & \dfrac{\partial f_1}{\partial x_2} \\ \dfrac{\partial f_2}{\partial x_1} & \dfrac{\partial f_2}{\partial x_2} \end{bmatrix} = \begin{bmatrix} \nabla f_1 \\ \nabla f_2 \end{bmatrix}. \tag{13}$$

At this point we notice that if the vector ∇f_1 is a scalar multiple of the vector ∇f_2, i.e., if ∇f_1 and ∇f_2 are parallel then the Jacobian (13) $\boldsymbol{J_f}$ is rank one. Therefore $\det(\boldsymbol{J_f}) = 0$, implying that there exists a zero eigenvalue with algebraic multiplicity one or two. Similarly, if $\nabla f_1 = 0$ or/and $\nabla f_2 = 0$ then $\det(\boldsymbol{J_f}) = 0$. □

In Figure 4 we provide a graphical illustration of Theorem 3 for saddle-node and pitchfork bifurcations. It is important to emphasize that the tangency condition of the nullclines mentioned in Theorem 3 is not necessary nor sufficient for a bifurcation to occur. In fact, ∇f_1 and ∇f_2 can be parallel at some fixed point and yet not generate any bifurcation.

Example: The nonlinear dynamical system

$$\begin{cases} \dot{x}_1 = x_1 x_2 - x_1^2 - x_1 \\ \dot{x}_2 = x_2 - x_1^2 - \mu \end{cases} \tag{14}$$

undergoes a *saddle-node bifurcation* at $\mu^* = 1.25$, and a *transcritical bifurcation* at $\mu^* = 1$. In Figure 5 we show the phase portraits of (14) as μ is varied within the range $[0.9, 1.35]$. The Jacobian of (14) is

$(x_1, x_2) = (0, 1)$ in Figure 5.

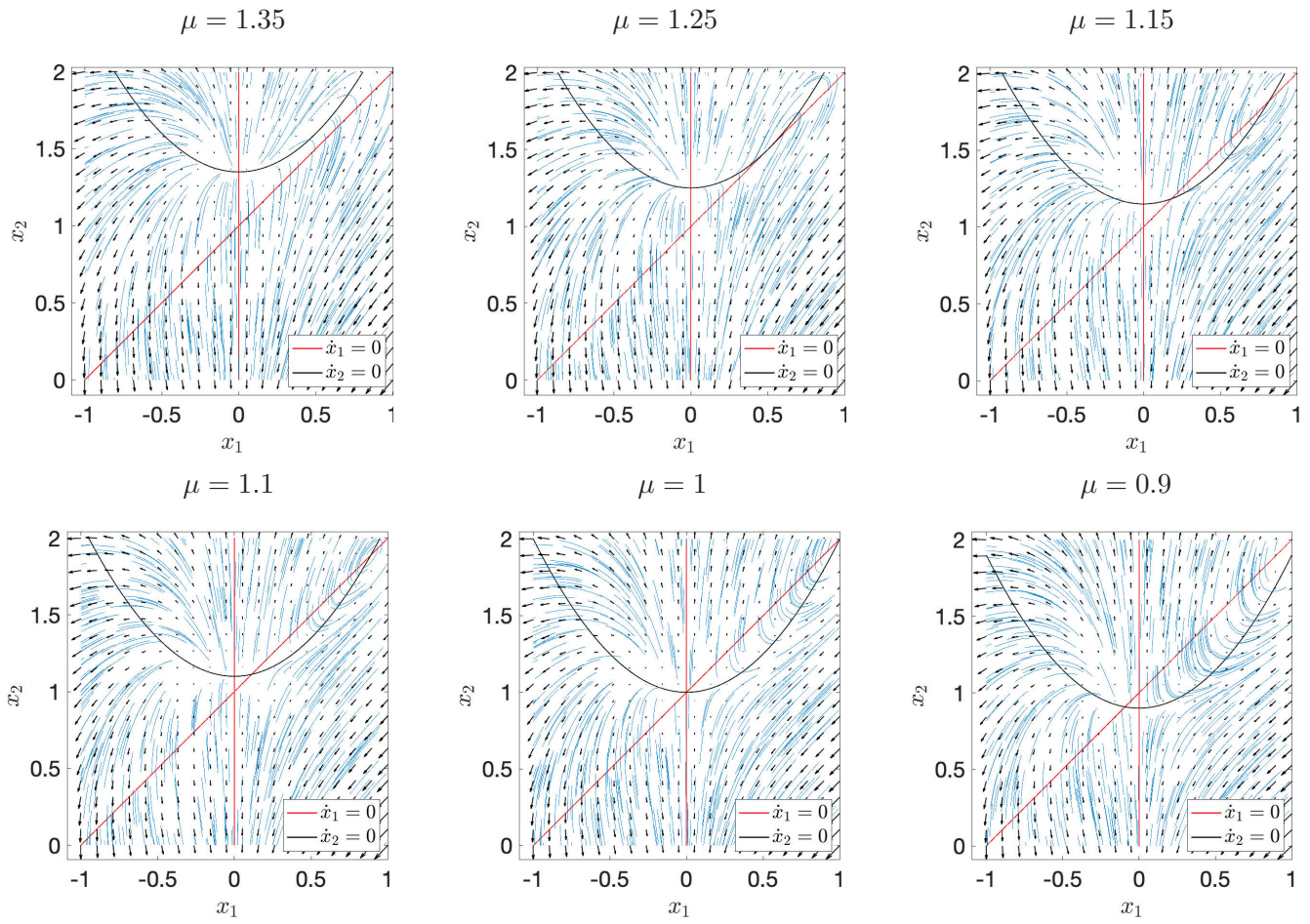

Figure 5: Phase portraits of the system (14) for different μ. For $\mu = 1.25$ the system undergoes a saddle node bifurcation at $\boldsymbol{x}_A = (0.5, 1.5)$. Note that for $\mu = 1.25$ the nullclines $\dot{x}_1 = 0$ and $\dot{x}_2 = 0$ are tangent at $\boldsymbol{x}_A$. For $\mu = 1$ the system undergoes a second zero-eigenvalue bifurcation at $\boldsymbol{x}_B^* = (0, 1)$. Such bifurcation is a transcritical bifurcation where two fixed points "exchange stability". At both bifurcation points there is a single real eigenvalue of the Jacobian crossing the imaginary axis with non-zero velocity .

$$\boldsymbol{J_f}(x_1, x_2) = \begin{bmatrix} x_2 - 2x_1 - 1 & x_1 \\ -2x_1 & 1 \end{bmatrix} \tag{15}$$

For $\mu_A^* = 5/4$ the system undergoes a *saddle-node bifurcation* at the fixed point

$$\boldsymbol{x}_A^* = \left(\frac{1}{2}, \frac{3}{2}\right). \tag{16}$$

Evaluating the Jacobian (15) at $(\boldsymbol{x}_A^*, \mu_A^*)$ yields

$$\boldsymbol{J_f}(\boldsymbol{x}_A^*) = \frac{1}{2}\begin{bmatrix} -1 & 1 \\ -2 & 2 \end{bmatrix}. \tag{17}$$

Hence, the two nullclines $\dot{x}_1 = 0$ and $\dot{x}_2 = 0$ are tangent at $\boldsymbol{x}_A^*$. Note, in fact, that that the rows of $\boldsymbol{J_f}(\boldsymbol{x}_B^*)$ (which represent the gradients of f_1 and f_2) are linearly dependent. The eigenvalues of (17) are

$$\lambda_1 = \frac{1}{2} \qquad \lambda_2 = 0. \tag{18}$$

As seen in Figure 5, as we decrease μ we have that the parabola representing the level set $\dot{x}_2 = 0$ translates downward, and the fixed point $\boldsymbol{x}_A^*$ splits into two (hyperbolic) fixed points. As we keep reducing μ, one

of the two fixed points that came out of the saddle node bifurcation heads towards the fixed point fixed point $\boldsymbol{x}^*(\mu) = (0, \mu)$. The Jacobian at $\boldsymbol{x}^*(\mu)$ is

$$\boldsymbol{J_f}(\boldsymbol{x}^*(\mu)) = \begin{bmatrix} \mu - 1 & 0 \\ 0 & 1 \end{bmatrix} \tag{19}$$

and has eigenvalues

$$\lambda_1(\mu) = \mu - 1 \qquad \lambda_2(\mu) = 1. \tag{20}$$

As seen in Figure 5, at $\mu = \mu_B^* = 1$ the fixed point $\boldsymbol{x}^*(\mu) = (0, \mu)$ collides with one of the two fixed point that came out of the saddle-node bifurcation. This yields another zero-eigenvalue bifurcation, i.e., a *transcritical bifurcation*. Note that at the transcritical bifurcation point

$$\boldsymbol{x}_B^* = (0, 1) \qquad \mu_B^* = 1 \tag{21}$$

the nullcline $\dot{x}_1 = 0$ intersects itself, and therefore the gradient ∇f_1 is zero at $\boldsymbol{x}_B^* = (0, 1)$, consistently with Theorem 3. The eigenvalues of $\boldsymbol{J_f}(\boldsymbol{x}_B^*)$ are $(\lambda_1, \lambda_2) = (0, 1)$.

Normal form of dynamical systems at zero-eigenvalue bifurcations. The normal form a dynamical system at zero eigenvalue bifurcations can be computed using the *normal form theorem* and the *local center manifold theorem* applied to the extended system (87) at the bifurcation point. The main steps are:

- Write the extended dynamical system (87) at bifurcation point $(\boldsymbol{x}^*, \mu^*)$ via the simple change of coordinates $\boldsymbol{\eta} = \boldsymbol{x}(t) - \boldsymbol{x}^*$, $r = \mu - \mu^*$.
- Expand the system at the bifurcation point as

$$\dot{\boldsymbol{\eta}} = \boldsymbol{J_f}(\boldsymbol{x}^*, \mu^*)\boldsymbol{\eta} + \boldsymbol{g}(\boldsymbol{\eta}, \mu^*), \tag{22}$$

  where $\boldsymbol{J_f}(\boldsymbol{x}^*, \mu^*)$ is the Jacobian at $(\boldsymbol{x}^*, \mu^*)$ and $\boldsymbol{g}$ represents the residual of the Taylor series. The spectral decomposition of $\boldsymbol{J_f}(\boldsymbol{x}^*, \mu^*)$ yields stable (V^c), unstable (V^u), and center (V^c) subspaces, and corresponding phase variables (see the course note 5).
- Compute the local center manifold of the extended system at the bifurcation point, and write the system in a normal form in the neighborhood of $(\boldsymbol{\eta}, r) = (\boldsymbol{0}, 0)$.

In Appendix A we provide two examples of calculation of normal forms in two-dimensional dynamical systems using this procedure. Specifically, we study a transcritical and a saddle-node bifurcation. The examples in Appendix A clearly demonstrate that by using local center manifolds analysis applied to the normal form of the extended dynamical system at the bifurcation point it is possible to characterize the zero-eigenvalue bifurcation in terms of a decoupled system that involves the center manifold and the stable/unstable manifolds. The bifurcation process develops entirely on the center manifold of the extended system. The dynamics on the stable/unstable manifolds is trivial. In Figure 6 we sketch the flow defined by the normal form of a two-dimensional dynamical systems that undergoes a saddle-node and supercritical pitchfork bifurcations.

The results obtained for the two-dimensional systems in Appendix A can be generalized to n-dimensional dynamical systems. For example, the normal form of a supercritical pitchfork bifurcation in a n-dimensional system is

$$\begin{cases} \dot{c} = cr - c^3 & \text{(center manifold)} \\ \dot{\boldsymbol{s}} = \boldsymbol{B}\boldsymbol{s} & \text{(stable subspace)} \\ \dot{\boldsymbol{u}} = \boldsymbol{C}\boldsymbol{u} & \text{(unstable subspace)} \end{cases} \tag{23}$$

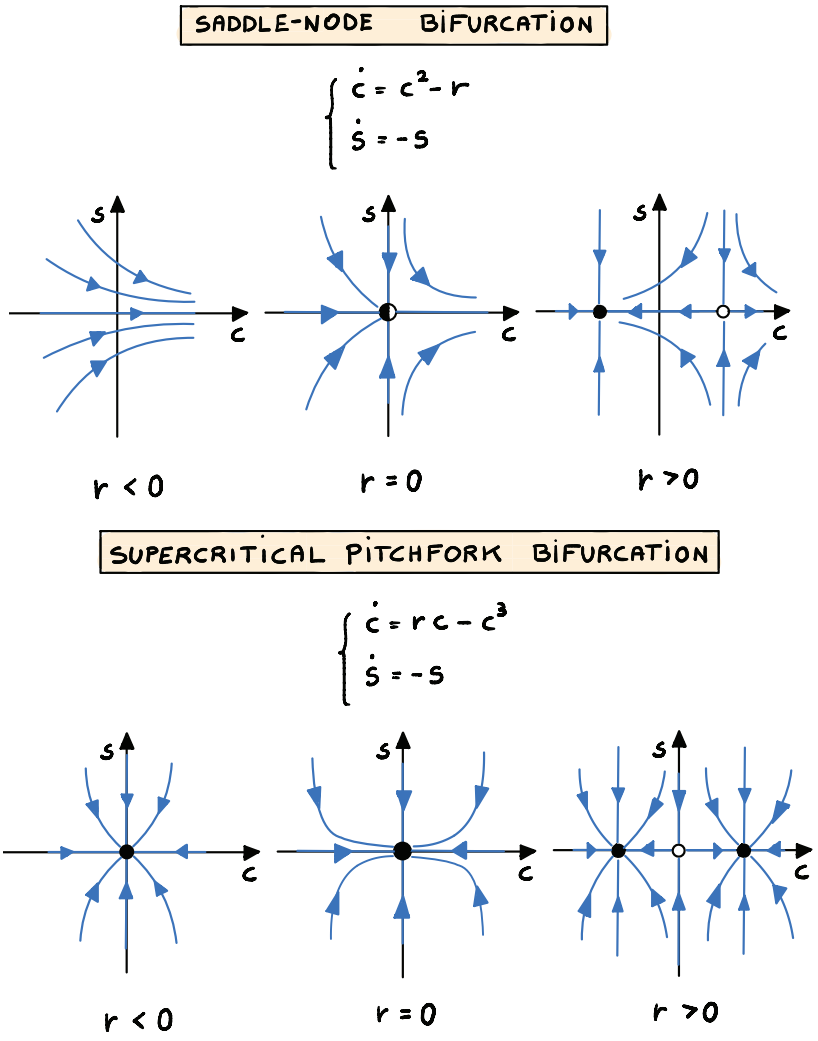

Figure 6: Normal form of two-dimensional saddle-node and supercritical pitchfork bifurcations. In these plots we assume that the bifurcation point is characterized by center (c variable) and stable (s variable) manifolds.

where $\boldsymbol{B}$ has eigenvalues with negative real part, and $\boldsymbol{C}$ has eigenvalues with positive real part.

In Figure 7 we provide an example of a thermal-fluid system that undergoes a supercritical pitchfork bifurcation at the onset of convective instability. The bifurcation diagram is computed numerically, and the type of bifurcation is identified using Sotomayor's Theorem 6.

Conditions for existence of saddle-node, transcritical, and pitchfork bifurcations. Is it possible to identify which type of zero-eigenvalue bifurcation takes place in an n-dimensional system without computing the normal form? The answer, is yes and the procedure is given in the following theorems due to Jorge Sotomayor.

Theorem 4 (Sotomayor's theorem for saddle-node bifurcations)**.** Suppose that the system (1) has a fixed point $(\boldsymbol{x}^*, \mu^*)$ satisfying the following conditions

a) $\boldsymbol{J_f}(\boldsymbol{x}^*, \mu^*)$ has a simple eigenvalue 0 with right eigenvector $\boldsymbol{v}$ and left eigenvector[6] $\boldsymbol{w}$, and k eigen-

[6]The left eigenvector of a square matrix $\boldsymbol{A}$ is a row vector such that $\boldsymbol{wA} = \lambda \boldsymbol{w}$. Taking the transpose, we see that the left

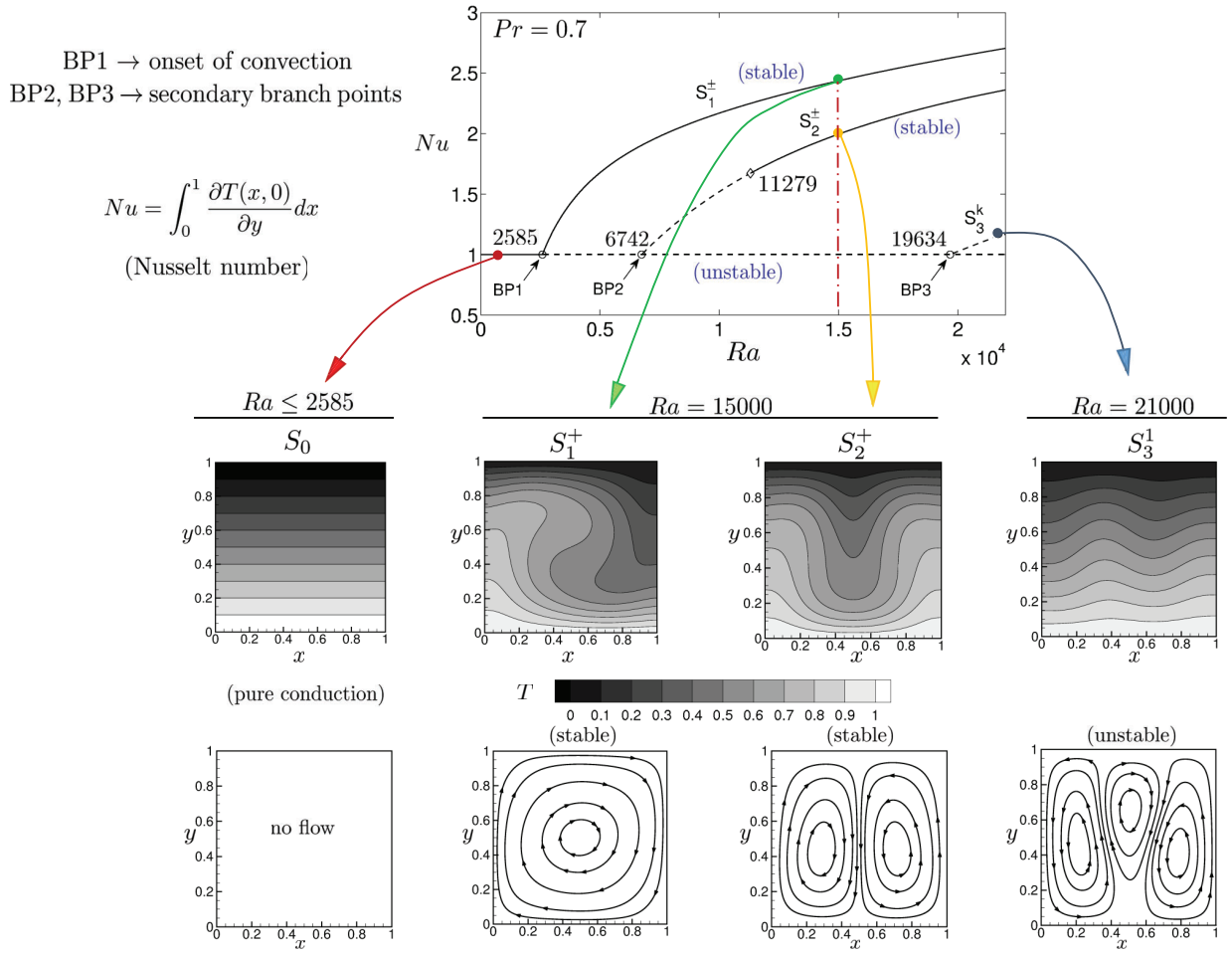

Figure 7: Onset of convective instability in a square cavity heated from below and cooled from above (isothermal horizontal walls), and adiabatic sidewalls. This fluid system transitions from a state of no-motion to a one-roll stable convection pattern via a supercritical pitchfork bifurcation. The bifurcation parameter is the Rayleigh number $Ra = g\beta L^3 \Delta T/(\nu\alpha)$. Here g is gravity, β is the isobaric compressibility of the fluid, L is the side length of the cavity, ΔT is the temperature difference between the horizontal walls, nu is the kinematic viscosity and α is the thermal diffusivity of the fluid.

values with negative real part,

b) $$\sum_{i=1}^{n} w_i \frac{\partial f_i(\boldsymbol{x}^*, \mu^*)}{\partial \mu} \neq 0,$$

c) $$\sum_{i=1}^{n} w_i \left[\sum_{l,p=1}^{n} \frac{\partial^2 f_i(\boldsymbol{x}^*, \mu^*)}{\partial x_l \partial x_p} v_l v_p \right] \neq 0.$$

Then there is a smooth curve of equilibrium points of (1) passing through $(\boldsymbol{x}^*, \mu^*)$. Depending on the signs of the expressions in b) and c), there are no equilibrium points of (1) near $\boldsymbol{x}^*$ when $\mu < \mu^*$ (or when $\mu > \mu^*$), and there are two fixed points points of (1) near when $\mu > \mu^*$ (or when $\mu < \mu^*$). The two fixed points are hyperbolic and have stable manifolds of dimensions k and $k+1$ respectively; i.e., the system (1) experiences a saddle-node bifurcation at the equilibrium point $\boldsymbol{x}^*$ as the parameter μ passes through the

eigenvector $\boldsymbol{A}$ is a right eigenvector of the matrix transpose $\boldsymbol{A}^T$.

bifurcation value $\mu = \mu^*$.

Example: Let us apply Theorem 4 to the system

$$\begin{cases} \dot{x}_1 = x_2 \\ \dot{x}_2 = x_2 - x_1^2 - \mu \end{cases} \tag{24}$$

As discussed in Appendix A, the Jacobian of (24) at $(\boldsymbol{x}^*, \mu^*) = (\boldsymbol{0}, 0)$

$$\boldsymbol{J_f}(\boldsymbol{0}, 0) = \begin{bmatrix} 0 & 1 \\ 0 & 1 \end{bmatrix} \tag{25}$$

has one zero eigenvalue $\lambda_1 = 0$ and one positive eigenvalue $\lambda_2 = 1$. The left and right eigenvectors corresponding to the zero eigenvalue are, respectively

$$\boldsymbol{v} = \begin{bmatrix} 1 \\ 0 \end{bmatrix}, \qquad \boldsymbol{w} = \begin{bmatrix} -1 \\ 1 \end{bmatrix}. \tag{26}$$

Let us now check if conditions b) and c) in Theorem 4 are satisfied.

$$\text{b)} \quad \sum_{i=1}^{2} w_i \frac{\partial f_i(\boldsymbol{0}, 0)}{\partial \mu} = 0 - 1 = -1 \neq 0, \tag{27}$$

$$\text{c)} \quad \sum_{i=1}^{2} w_i \left[\sum_{l,p=1}^{2} \frac{\partial^2 f_i(\boldsymbol{0}, 0)}{\partial x_l \partial x_p} v_l v_p \right] = -2 \neq 0. \tag{28}$$

Hence, the system (24) undergoes a saddle node bifurcation at $(\boldsymbol{x}^*, \mu^*) = (\boldsymbol{0}, 0)$.

Theorem 5 (Sotomayor's theorem for transcritical bifurcations)**.** Suppose that the system (1) has a fixed point $(\boldsymbol{x}^*, \mu^*)$ for which the following conditions are satisfied:

a) $\boldsymbol{J_f}(\boldsymbol{x}^*, \mu^*)$ has a simple eigenvalue 0 with right eigenvector $\boldsymbol{v}$ and left eigenvector $\boldsymbol{w}$,

b) $\displaystyle\sum_{i=1}^{n} w_i \frac{\partial f_i(\boldsymbol{x}^*, \mu^*)}{\partial \mu} = 0$, c) $\displaystyle\sum_{i=1}^{n} w_i \left[\sum_{l=1}^{n} \frac{\partial f_i(\boldsymbol{x}^*, \mu)}{\partial \mu \partial x_l} v_l \right] \neq 0$, d) $\displaystyle\sum_{i=1}^{n} w_i \left[\sum_{l,p=1}^{n} \frac{\partial^2 f_i(\boldsymbol{x}^*, \mu)}{\partial x_l \partial x_p} v_l v_p \right] \neq 0$.

Then the system (1) undergoes a transcritical bifurcation at the equilibrium point $\boldsymbol{x}^*$ as the parameter μ varies through the bifurcation value μ^*.

Example: Let us apply Theorem 5 to the system

$$\begin{cases} \dot{x}_1 = x_2 \\ \dot{x}_2 = -x_2 + \mu x_1 - x_1^2 \end{cases} \tag{29}$$

As discussed in Appendix A, the Jacobian of (29) at $(\boldsymbol{x}^*, \mu^*) = (\boldsymbol{0}, 0)$

$$\boldsymbol{J_f}(\boldsymbol{0}, 0) = \begin{bmatrix} 0 & 1 \\ 0 & 1 \end{bmatrix} \tag{30}$$

has one zero eigenvalue $\lambda_1 = 0$ and one negative eigenvalue $\lambda_2 = -1$ The left and right eigenvectors corresponding to $\lambda_1 = 0$ are, respectively

$$\boldsymbol{v} = \begin{bmatrix} 1 \\ 0 \end{bmatrix}, \qquad \boldsymbol{w} = \begin{bmatrix} -1 \\ 1 \end{bmatrix}. \tag{31}$$

Let us now check if conditions b), c) and d) in Theorem 5 are satisfied.

$$\text{b)} \quad \sum_{i=1}^{n} w_i \frac{\partial f_i(\mathbf{0},0)}{\partial \mu} = 0, \tag{32}$$

$$\text{c)} \quad \sum_{i=1}^{n} w_i \left[\sum_{l=1}^{2} \frac{\partial^2 f_i(\mathbf{0},0)}{\partial \mu \partial x_l} v_l \right] = 1 \neq 0, \tag{33}$$

$$\text{d)} \quad \sum_{i=1}^{n} w_i \left[\sum_{l,p=1}^{2} \frac{\partial^2 f_i(\boldsymbol{x}^*,\mu^*)}{\partial x_l \partial x_p} v_l v_p \right] = -1 \neq 0. \tag{34}$$

Hence, (29) undergoes a transcritical bifurcation at $(\boldsymbol{x}^*,\mu^*) = (\mathbf{0},0)$.

Theorem 6 (Sotomayor's theorem for pitchfork bifurcations)**.** Suppose that the system (1) has a fixed point $(\boldsymbol{x}^*,\mu^*)$ for which the following conditions are satisfied:

a) $\boldsymbol{J_f}(\boldsymbol{x}^*,\mu^*)$ has a simple eigenvalue 0 with right eigenvector $\boldsymbol{v}$ and left eigenvector $\boldsymbol{w}$.

b) $\displaystyle\sum_{i=1}^{n} w_i \frac{\partial f_i(\boldsymbol{x}^*,\mu^*)}{\partial \mu} = 0,$ c) $\displaystyle\sum_{i=1}^{n} w_i \left[\sum_{l=1}^{n} \frac{\partial f_i(\boldsymbol{x}^*,\mu)}{\partial \mu \partial x_l} v_l \right] \neq 0,$

d) $\displaystyle\sum_{i=1}^{n} w_i \left[\sum_{l,p=1}^{n} \frac{\partial^2 f_i(\boldsymbol{x}^*,\mu)}{\partial x_l \partial x_p} v_l v_p \right] = 0,$ e) $\displaystyle\sum_{i=1}^{n} w_i \left[\sum_{l,p,q=1}^{n} \frac{\partial^3 f_i(\boldsymbol{x}^*,\mu)}{\partial x_l \partial x_p \partial x_q} v_l v_p v_q \right] \neq 0.$

Then the system (1) undergoes a pitchfork bifurcation at the equilibrium point $\boldsymbol{x}^*$ as the parameter μ varies through the bifurcation value μ^*.

Theorem 6 was used to identify the pitchfork bifurcation in the high-dimensional nonlinear dynamical system discussed in Figure 7.

Hopf bifurcation. So far we studied bifurcations of equilibria characterized by a single real eigenvalue crossing the imaginary axis as a real parameter μ is varied. We called such bifurcations *zero eigenvalue bifurcations*, and studied their properties using center-manifold theory applied to the extended system (87). At the beginning of this course note we emphasized that local bifurcations of equilibria can occur at any non-hyperbolic fixed point (see, e.g., Peixoto's theorem 1 on the structural stability of two-dimensional systems). Hence, it is natural to ask what happens to an equilibrium point $\boldsymbol{x}(\mu)$ if the Jacobian $J_{\boldsymbol{f}}(\boldsymbol{x}^*(\mu),\mu)$ has a pair of complex conjugate eigenvalues $\lambda_{1,2}(\mu)$ crossing the imaginary axis with nonzero velocity $d\lambda_{1,2}(\mu)/d\mu \neq 0$ as μ is varied (see Figure 8).

In this case the system undergoes a *Hopf bifurcation*. Such bifurcation is not characterized by fixed points merging together or branching out of a fixed point, but rather by a local change of stability that yields the creation or annihilation of a *limit cycle* surrounding the fixed point. The normal form theorem gives us all required information about the structure of the local center manifold in a neighborhood of a Hopf bifurcation point.

Theorem 7 (Hopf bifurcation (1942))**.** Suppose that the system (1) has a fixed point $(\boldsymbol{x}^*,\mu^*)$ at which the following properties are satisfied:

a) The Jacobian matrix $\boldsymbol{J_f}(\boldsymbol{x}^*,\mu^*)$ has a pair of pure imaginary eigenvalues $\lambda_{1,2}(\mu^*) = \pm\omega i$ and no other eigenvalues with zero real part[7].

[7] If condition a) in Theorem 7 is satisfied then there exists a smooth curve $\boldsymbol{x}^*(\mu)$ representing the location of the fixed point

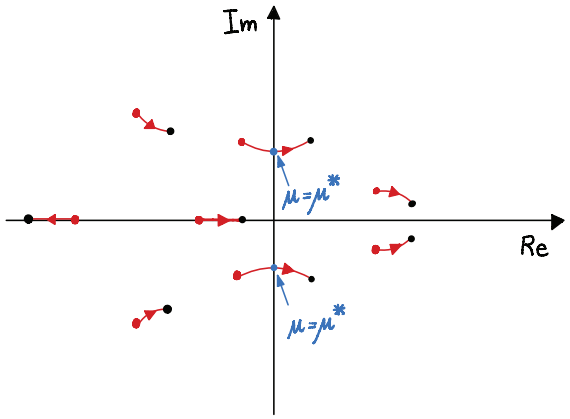

Figure 8: Hopf bifurcations are characterized by a pair of complex conjugate eigenvalues crossing the imaginary axis with non-zero velocity. Shown is a sketch of the eigenvalues of the Jacobain matrix $J_{\boldsymbol{f}}(\boldsymbol{x}^*(\mu),\mu)$ evaluated at the fixed point $\boldsymbol{x}^*(\mu)$. As μ is varied the eigenvalues move from the red dots to the black dots. At $\mu=\mu^*$ one we have a pair of imaginary eigenvalues and no other eigenvalue with zero real part.

b) The complex conjugate eigenvalues $\lambda_{1,2}(\mu)$ cross the imaginary axis with non-zero "velocity"

$$\frac{d\,\mathrm{Re}\,[\lambda_{1,2}(\mu^*)]}{d\mu}=D\neq 0. \tag{35}$$

Then there exists a unique three-dimensional center manifold passing through $(\boldsymbol{x}^*,\mu^*)$ and a smooth coordinates system for which the Taylor expansion of degree 3 on the center manifold is given by

$$\begin{cases}\dot{R}=rDR+AR^3+\mathcal{O}(r^2R,rR^3,R^5)\\ \dot{\vartheta}=\omega+rC+BR^2+\mathcal{O}(r^2,rR^2,R^4)\end{cases} \tag{36}$$

where

$$C=\frac{d\,\mathrm{Im}[\lambda_{1,2}(\mu^*)]}{d\mu}, \tag{37}$$

$r=\mu-\mu^*$ is the transformed bifurcation parameter ($r=0$ corresponds to $\mu=\mu^*$), (R,ϑ) are polar coordinates, D is given in (35), and A and B are constants that depend on the system.

The system (36) can be written in local Cartesian coordinates as

$$\begin{cases}\dot{c}_1=rDc_1-(\omega+rC)c_2+Ac_1(c_1^2+c_2^2)-Bc_2(c_1^2+c_2^2)+\cdots\\ \dot{c}_2=(\omega+rC)c_1+rDc_2+Bc_1(c_1^2+c_2^2)-Ac_2(c_1^2+c_2^2)+\cdots\end{cases} \tag{38}$$

(see Appendix B for the derivation).

Existence of limit cycles. The normal form (36) appearing in Hopf's bifurcation Theorem 7 implies that for $A\neq 0$[8] there exists a limit cycle surrounding the fixed point located at $R=0$. Note that the fixed point at $R=0$ in normal coordinates corresponds to some fixed point $\boldsymbol{x}^*(\mu)$ in Cartesian coordinates.

as a function of μ in a neighborhood of μ^*. The existence of such smooth curve follows immediately from the implicit function Theorem 2.

[8] If $A=0$ the Taylor expansion in (36) is insufficient to describe the system. This implies that if $A=0$ then we need to add more terms.

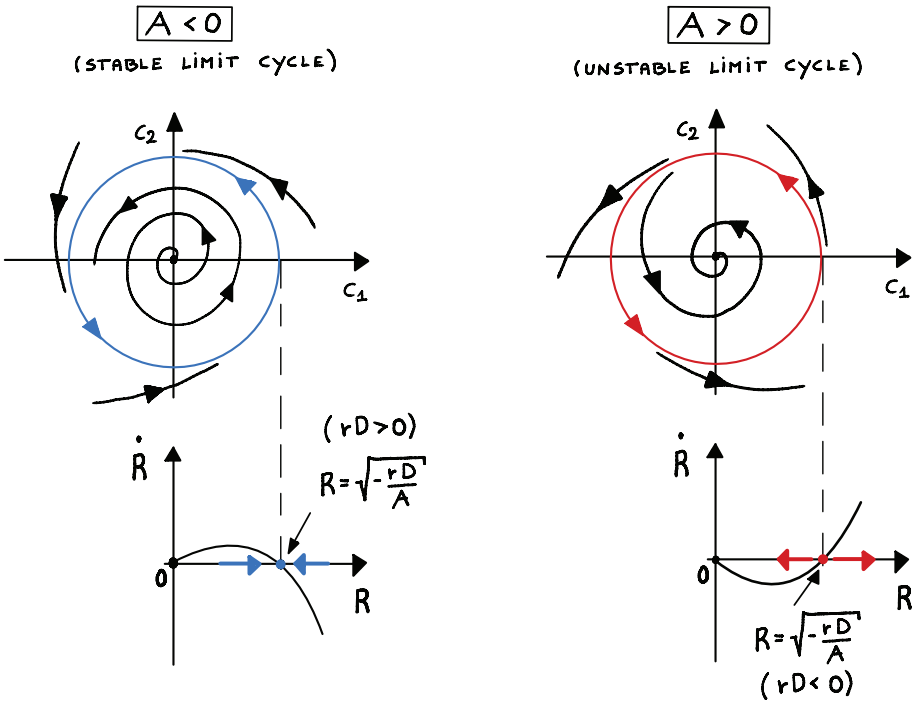

Figure 9: Stable and unstable limit cycles associated with a supercritical and a subcritical Hopf bifurcation in normal coordinates.

In fact, the analysis of the Hopf bifurcation is performed by setting up a local coordinate system that is constantly sitting at the fixed point, very much in the same way as in (22).

Setting $\dot{R} = 0$ in (36) yields two equilibrium solutions

$$R = 0 \quad \text{(fixed point)}, \qquad \text{and} \qquad R = \sqrt{-\frac{rD}{A}} \quad \text{(limit cycle)}. \tag{39}$$

The solution to the second equation at $R = \sqrt{-rD/A}$ is easily obtained as

$$\vartheta(t) = \vartheta_0 + \left(\omega + rC - r\frac{BD}{A}\right) t. \tag{40}$$

Hence, the Hopf bifurcation yields a limit cycle the radius of which is grows like the square root of the bifurcation parameter r The analysis of the vector field

$$\dot{R} = rDR + AR^3 \tag{41}$$

allows us to study the stability of the limit cycle (see Figure 9). Specifically, we see that

- for $A > 0$ the limit cycle is unstable and it exists for $rD < 0$,
- for $A < 0$ the limit cycle is stable and it exists for $rD > 0$.

Supercritical and subcritical Hopf bifurcations. Depending on the sign of the parameter A in (36), (38) and (41) we can have two different types of Hopf bifurcations, namely

- a *supercritical Hopf bifurcation* for $A < 0$,
- a *subcritical Hopf bifurcation* for $A > 0$.

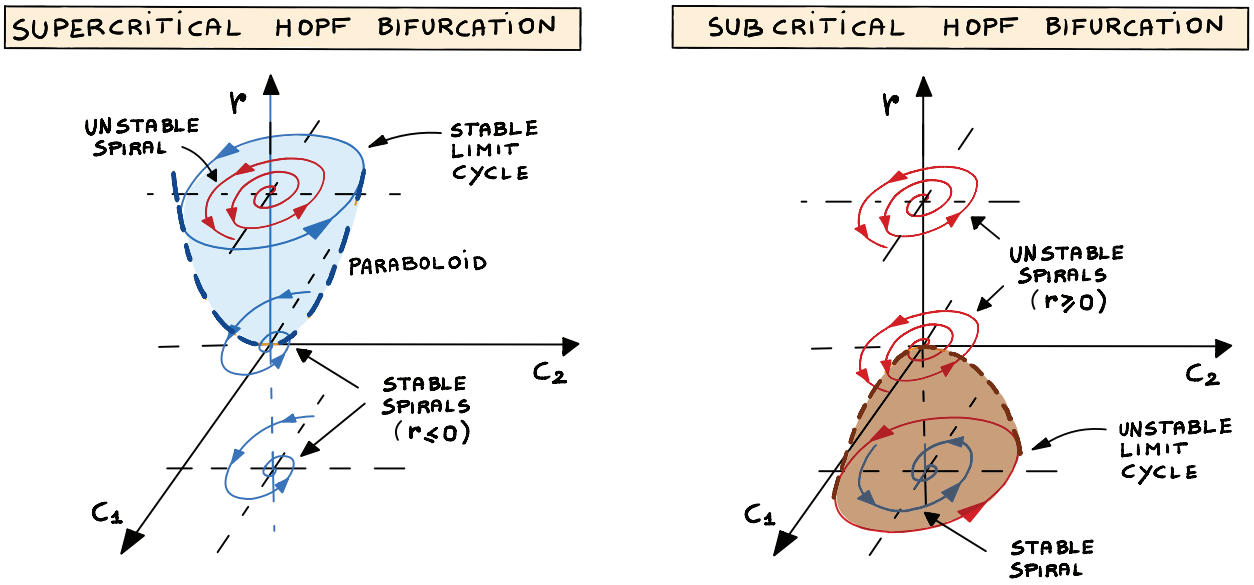

Figure 10: Supercritical ($A < 0$) and subcritical ($A > 0$) Hopf bifurcations on the three dimensional center manifold mentioned in Theorem 7.

To understand these two bifurcations it is convenient to set $D = 1$ (complex conjugate eigenvalues are crossing the imaginary axis from left to right with velocity one as μ increases) and $C = 0$ in (36). This yields the simplified system

$$\begin{cases} \dot{R} = rR + AR^3 + \cdots \\ \dot{\vartheta} = \omega + BR^2 + \cdots \end{cases} \tag{42}$$

The phase portraits of the system (42) are sketched in Figure 10 for different values of μ, and different A.

It is important to emphasize that the direction in which the complex conjugate eigenvalues cross the imaginary axis during the bifurcation process do *not* identify the type of Hopf bifurcation. In other words, it is possible to have a supercritical Hopf bifurcation with complex conjugate eigenvalues crossing the imaginary axis from left to right or from right to left. Similarly it is possible to have a subcritical Hopf bifurcation with complex with complex conjugate eigenvalues crossing the imaginary axis from left to right or from right to left. This symmetry is due to the fact that the radius of the limit defined by (39) depends on the product rD, where D represents the velocity (with sign) by which the eigenvalues are crossing the imaginary axis (see Eq. (35)).

Supercritical Hopf bifurcations are usually associated with transitions from steady states/equilibria to periodic states. In Figure 11 we show one of such transition in a high-dimensional fluid system described by the Navier-Stokes equations (incompressible fluid flow past a circular cylinder).

Hopf bifurcations in two-dimensional systems. For large systems of equations, computation of the normal form (36) and the cubic coefficient A, which determines the stability of the limit cycle, can be a substantial undertaking. However, for two-dimensional systems the calculation of A is not too difficult, and can be done directly by writing the system at the bifurcation point in a canonical form shown below (Eq. (49)), and then using center manifold theory. To this end, consider the system (10), and suppose that there exits a fixed point $\boldsymbol{x}^*(\mu)$ with Jacobian that has two complex conjugate eigenvalues crossing the imaginary axis at $\mu = \mu^*$ with nonzero velocity. How do we figure out what kind of Hopf bifurcation is taking place? As we know, this is determined by the value of the parameter A in (36). To determine such

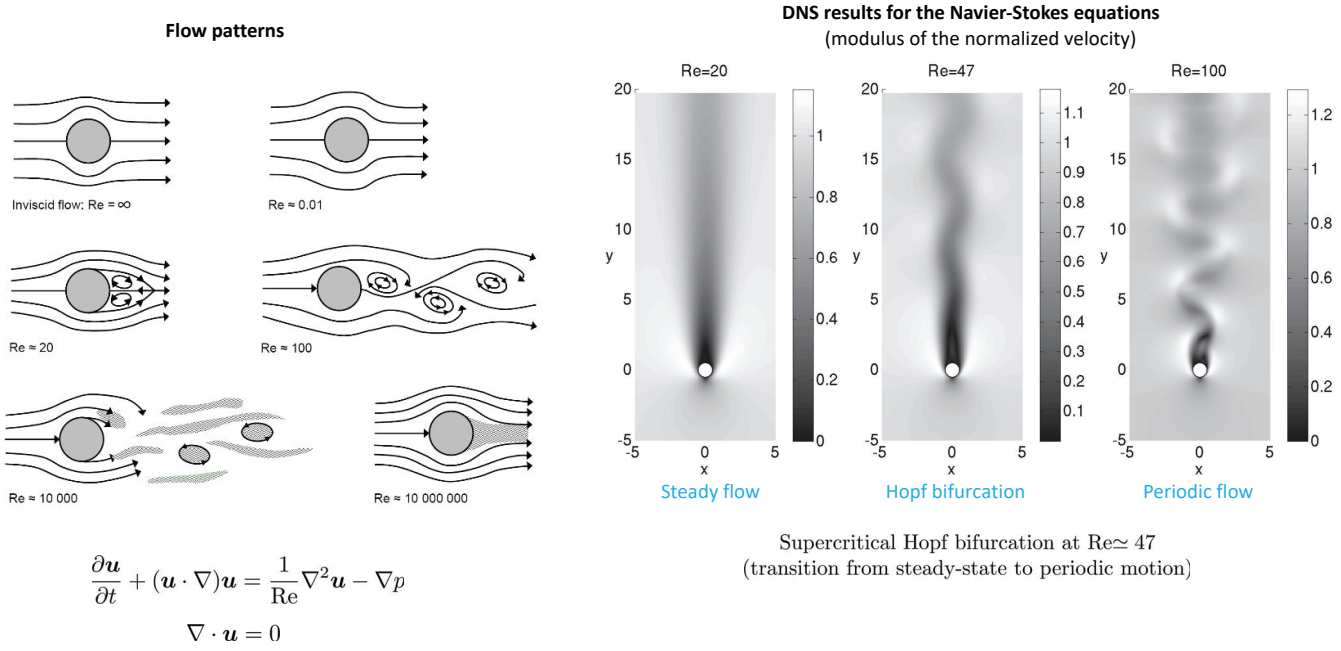

$$\frac{\partial \boldsymbol{u}}{\partial t} + (\boldsymbol{u}\cdot\nabla)\boldsymbol{u} = \frac{1}{\mathrm{Re}}\nabla^2\boldsymbol{u} - \nabla p$$
$$\nabla\cdot\boldsymbol{u} = 0$$

Figure 11: Transition from steady flow to periodic flow (Von-Karman periodic wake wake past a cylinder) via a supercritical Hopf bifurcation at $Re = 47$ in a fluid system. In this application, the bifurcation parameter is the Reynolds number $Re = \delta U/\nu$ of the flow, which depends on the cylinder diameter δ, the upstream fluid velocity U, and the kinematic viscosity of the fluid ν.

parameter, let us first write the system

$$\begin{cases} \dot{x}_1 = f_1(x_1, x_2, \mu) \\ \dot{x}_2 = f_2(x_1, x_2, \mu) \end{cases} \tag{43}$$

in a normal form. To this end, we first change the coordinates and rewrite the system at the Hopf bifurcation point $(\boldsymbol{x}^*, \mu^*)$ as

$$\frac{d\boldsymbol{\eta}}{dt} = \boldsymbol{J_f}(\boldsymbol{x}^*(\mu^*), \mu^*)\boldsymbol{\eta} + \boldsymbol{g}(\boldsymbol{\eta}, \mu^*), \tag{44}$$

where

$$\boldsymbol{\eta} = \boldsymbol{X}(t, \boldsymbol{x}_0) - \boldsymbol{x}^*(\mu^*). \tag{45}$$

The Jacobian matrix $\boldsymbol{J_f}(\boldsymbol{x}^*(\mu^*), \mu^*)$ has a pair of imaginary eigenvalues of the form

$$\lambda_{1,2} = \pm\omega i, \tag{46}$$

where ω is a real number (positive or negative). By computing the *real Jordan form*[9] of $\boldsymbol{J_f}(\boldsymbol{x}^*(\mu^*), \mu^*)$ and the corresponding similarity transformation $\boldsymbol{P}$ defined by the real and imaginary parts of one eigenvector (see Appendix A in the course note 5) we can change the variables as

$$\boldsymbol{q} = \boldsymbol{P}^{-1}\boldsymbol{\eta}. \tag{48}$$

[9]The real Jordan form of a 2×2 matrix $\boldsymbol{J}$ with complex conjugate eigenvalues $\lambda_{1,2} = \pm i\omega$ is

$$\boldsymbol{K} = \begin{bmatrix} 0 & \pm\omega \\ \mp\omega & 0 \end{bmatrix}. \tag{47}$$

The similarity transformation $\boldsymbol{P}$ that takes the matrix $\boldsymbol{J}$ into the skew symmetric matrix $\boldsymbol{K} = \boldsymbol{P}\boldsymbol{J}\boldsymbol{P}^{-1}$ has the real and the imaginary parts of one eigenvector of $\boldsymbol{J}$ as columns.

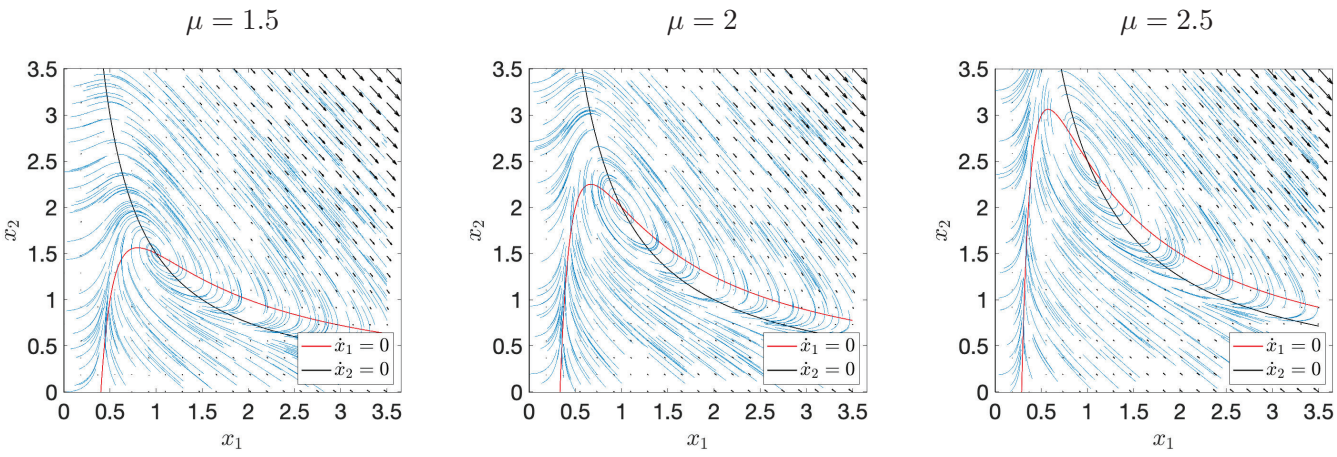

Figure 12: Phase portraits of the system (51) for different μ. The system undergoes a supercritical Hopf bifurcation at $\boldsymbol{x}^* = (1, 2)$ for $\mu^* = 2$.

and transform the dynamical system (44) into the standard form

$$\begin{cases} \dfrac{dq_1}{dt} = \omega q_2 + H_1(q_1, q_2) \\ \dfrac{dq_2}{dt} = -\omega q_1 + H_2(q_1, q_2) \end{cases} \tag{49}$$

where ω can be positive or negative. The coefficient A appearing in (36) can be now expressed in terms of H_1, H_2 and ω by the formula[10]

$$\begin{aligned} A = &\frac{1}{16}\left[\frac{\partial^3 H_1}{\partial q_1^3} + \frac{\partial^3 H_1}{\partial q_1 \partial q_2^2} + \frac{\partial^3 H_2}{\partial q_1^2 \partial q_2} + \frac{\partial^3 H_2}{\partial q_2^3}\right] + \\ &\frac{1}{16\omega}\left[\frac{\partial^2 H_1}{\partial q_1 \partial q_2}\left(\frac{\partial^2 H_1}{\partial q_1^2} + \frac{\partial^2 H_1}{\partial q_2^2}\right) - \frac{\partial^2 H_2}{\partial q_1 \partial q_2}\left(\frac{\partial^2 H_2}{\partial q_1^2} + \frac{\partial^2 H_2}{\partial q_2^2}\right) - \right. \\ &\left. \frac{\partial^2 H_1}{\partial q_1^2}\frac{\partial^2 H_2}{\partial q_1^2} + \frac{\partial^2 H_1}{\partial q_2^2}\frac{\partial^2 H_2}{\partial q_2^2}\right], \end{aligned} \tag{50}$$

where all derivatives of $H_1(q_1, q_2)$ and $H_2(q_1, q_2)$ are evaluated at $(0, 0)$.

Example: The nonlinear dynamical system

$$\begin{cases} \dot{x}_1 = 1 - (\mu + 1)x_1 + x_1^2 x_2 \\ \dot{x}_2 = \mu x_1 - x_1^2 x_2 \end{cases} \tag{51}$$

undergoes a supercritical Hopf bifurcation at $\boldsymbol{x}^* = (1, 2)$ for $\mu^* = 2$. To show this, let us first notice that the system has only one fixed point located at

$$\boldsymbol{x}^*(\mu) = (1, \mu), \tag{52}$$

(see Figure 12). The Jacobian of (51) is

$$J_{\boldsymbol{f}}(\boldsymbol{x}, \mu) = \begin{bmatrix} -(\mu + 1) + 2x_1 x_2 & x_1^2 \\ \mu - 2x_1 x_2 & -x_1^2 \end{bmatrix}. \tag{53}$$

[10]The proof of (50) is given in the book by Guckenheimer and Holmes, "Nonlinear oscillations, dynamical systems and bifurcations of vector fields" at page 154.

Evaluating (53) at the fixed point (52) yields

$$J_{\boldsymbol{f}}(\boldsymbol{x}^*(\mu),\mu) = \begin{bmatrix} \mu-1 & 1 \\ -\mu & -1 \end{bmatrix}. \tag{54}$$

The eigenvalues of $J_{\boldsymbol{f}}(\boldsymbol{x}^*(\mu),\mu)$ are

$$\lambda_{1,2}(\mu) = \frac{(\mu-2) \pm \sqrt{(\mu-2)^2-4}}{2}. \tag{55}$$

Clearly, at $\mu^* = 2$ the complex conjugate eigenvalues (55) cross the imaginary axis (from left to right as μ increases) with nonzero velocity

$$D = \left.\frac{d\,\mathrm{Re}(\lambda_{1,2}(\mu))}{d\mu}\right|_{\mu=\mu^*} = \frac{1}{2}. \tag{56}$$

Therefore there is Hopf bifurcation at $\boldsymbol{x}^*(\mu^*) = (1,2)$, $\mu^* = 2$. Which one? Subcritical or supercritical? To answer this question, we rewrite the system (51) at the fixed point (52). This is achieved by shifting the phase variables as

$$\boldsymbol{\eta}(t) = \boldsymbol{x}(t) - \boldsymbol{x}^*(\mu), \tag{57}$$

i.e.,

$$\eta_1 = x_1 - 1 \qquad \eta_2 = x_2 - \mu, \tag{58}$$

and expanding the system in the new variables at $(1,\mu)$ via Taylor theorem. A substitution of (58) into (51) yields

$$\begin{cases} \dot{\eta}_1 = (\mu-1)\eta_1 + \eta_2 + \eta_1^2\eta_2 + 2\eta_1\eta_2 + \mu\eta_1^2 \\ \dot{\eta}_2 = -\mu\eta_1 - \eta_2 - \eta_1^2\eta_2 - 2\eta_1\eta_2 - \mu\eta_1^2 \end{cases} \tag{59}$$

At the bifurcation $\mu^* = 2$ point we have

$$\begin{cases} \dot{\eta}_1 = \eta_1 + \eta_2 + \eta_1^2\eta_2 + 2\eta_1\eta_2 + 2\eta_1^2 \\ \dot{\eta}_2 = -2\eta_1 - \eta_2 - \eta_1^2\eta_2 - 2\eta_1\eta_2 - 2\eta_1^2 \end{cases} \tag{60}$$

This system can be written in the form (45), i.e.,

$$\dot{\boldsymbol{\eta}} = \boldsymbol{J}_{\boldsymbol{f}}(\boldsymbol{x}^*(\mu^*),\mu^*)\boldsymbol{\eta} + \boldsymbol{g}(\boldsymbol{\eta},\mu^*), \tag{61}$$

where

$$\boldsymbol{J}_{\boldsymbol{f}}(\boldsymbol{x}^*(\mu^*),\mu^*) = \begin{bmatrix} 1 & 1 \\ -2 & -1 \end{bmatrix} \tag{62}$$

is the Jacobian (54) evaluated at $\mu^* = 2$, and

$$g_1(\boldsymbol{\eta},\mu^*) = \eta_1^2\eta_2 + 2\eta_1\eta_2 + 2\eta_1^2, \qquad g_2(\boldsymbol{\eta},\mu^*) = -\eta_1^2\eta_2 - 2\eta_1\eta_2 - 2\eta_1^2. \tag{63}$$

The real Jordan form of (62) is

$$\begin{bmatrix} 0 & -1 \\ 1 & 0 \end{bmatrix} = \underbrace{\begin{bmatrix} 1 & 0 \\ -1 & -1 \end{bmatrix}}_{\boldsymbol{P}} \underbrace{\begin{bmatrix} 1 & 1 \\ -2 & -1 \end{bmatrix}}_{\boldsymbol{J}_{\boldsymbol{f}}(\boldsymbol{x}^*(\mu^*),\mu^*)} \underbrace{\begin{bmatrix} 1 & 0 \\ -1 & -1 \end{bmatrix}}_{\boldsymbol{P}^{-1}}. \tag{64}$$

The matrix $\boldsymbol{P}$ has the real and the imaginary part of one eigenvector of $\boldsymbol{J}_{\boldsymbol{f}}(\boldsymbol{x}^*(\mu^*),\mu^*)$ as columns, and it defines a transformation between $\boldsymbol{\eta}$ and new set of variables $\boldsymbol{q}$ as (see equation (48))

$$\boldsymbol{q} = \boldsymbol{P}^{-1}\boldsymbol{\eta}, \tag{65}$$

i.e.,

$$\eta_1 = q_1, \qquad \eta_2 = -q_1 - q_2. \tag{66}$$

Such a transformation allows us to write the system (61) in the form (49) as

$$\begin{cases} \dfrac{dq_1}{dt} = -q_2 + H_1(q_1, q_2) \\ \dfrac{dq_2}{dt} = q_1 + H_2(q_1, q_2) \end{cases} \tag{67}$$

where

$$H_1(q_1, q_2) = -q_1^3 - q_1^2 q_2 - 2q_1 q_2, \qquad H_2(q_1, q_2) = q_1^3 + q_1^2 q_2 + 2q_1 q_2 = -H_1(q_1, q_2). \tag{68}$$

At this point we can evaluate the coefficient (50). The only nonzero terms are

$$A = \frac{1}{16}\left[\frac{\partial^3 H_1}{\partial q_1^3} + \frac{\partial^3 H_2}{\partial q_1^2 \partial q_2}\right] = \frac{1}{16}\left[-6 + 1\right] = -\frac{5}{16}. \tag{69}$$

Hence, the fixed point (52) undergoes a *supercritical* Hopf bifurcation at $\mu^* = 2$. This implies that there exist a stable limit cycle surrounding the fixed point $\boldsymbol{x}^*(\mu) = (1, \mu)$ for $\mu > 2$.

Bifurcations depending on multiple parameters. There are many other bifurcations of equilibria that can take place in dynamical systems. Some of these bifurcations are characterized by multiple parameters. For instance,

- **Bogdanov-Takens bifurcation.** The Bogdanov-Takens bifurcation is a local bifurcation of an equilibrium point at which the Jacobian of the system has a zero eigenvalue of algebraic multiplicity two (see the book of Gukenheimer and Holmes, Section 7.3). The bifurcation depends on two parameters. For nearby parameter values, the system has two equilibria (a saddle and a nonsaddle) which collide and disappear via a saddle-node bifurcation. The nonsaddle equilibrium undergoes an Andronov-Hopf bifurcation generating a limit cycle. This cycle degenerates into an orbit homoclinic to the saddle and disappears via a saddle homoclinic bifurcation.
- **Saddle-node Hopf bifurcation.** The saddle-node Hopf bifurcation is a bifurcation of an equilibrium point in a two-parameter family of autonomous ODEs at which the Jacobian of the system has a zero eigenvalue and a pair of purely imaginary eigenvalues. This bifurcation is described in the book of Gukenheimer and Holmes, Section 7.4.

Appendix A: Calculation of the normal form of zero-eigenvalue bifurcations in 2D

In this Appendix we provide a detailed calculation of the normal form of two zero-eigenvalue bifurcations (transcritical and saddle node) arising in two-dimensional dynamical systems. In particular, The procedure can is general and it can be applied to other zero eigenvalue bifurcations.

Transcritical bifurcation. Consider the two-dimensional system

$$\begin{cases} \dot{x}_1 = x_2 \\ \dot{x}_2 = -x_2 + \mu x_1 - x_1^2 \end{cases} \tag{70}$$

In Figure 13 we plot phase portraits of the system (70) for different μ. The system has two fixed points

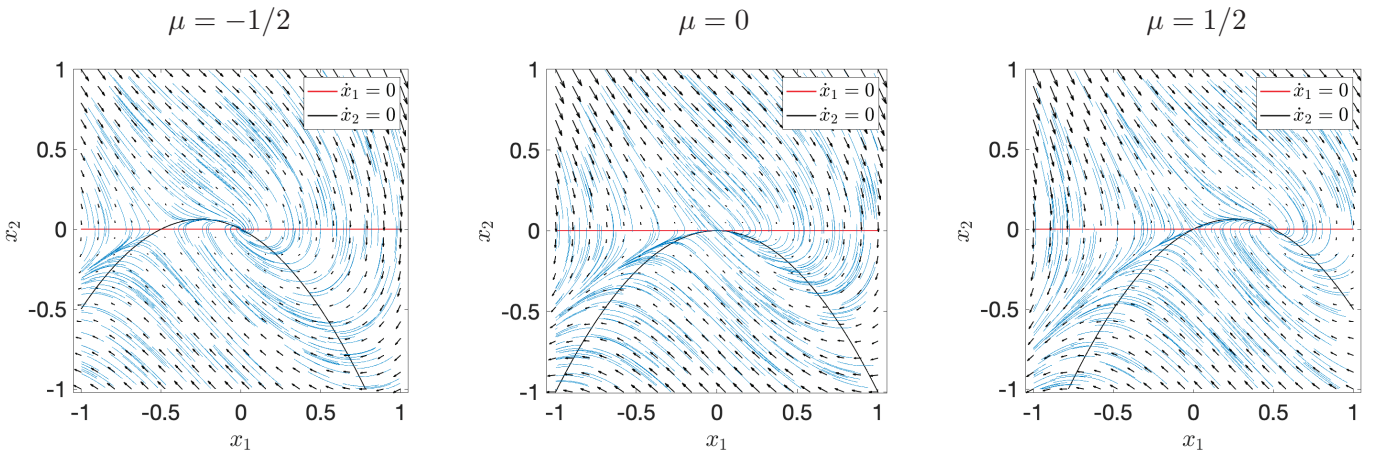

Figure 13: Phase portraits of the system (70) for different μ. Note that the system seems to have a spiral before and after the bifurcation, but actually when μ approaches zero such spiral becomes a stable node as predicted by the normal form in Figure 15. Note also that since the bifurcation is local we have that index is preserved before and after the bifurcation. In other word, the index of the non-hyperbolic fixed point at $(x_1, x_2, \mu) = (0, 0, 0)$ is zero (saddle node + attractor).

located at

$$\boldsymbol{x}_A^* = (0, 0) \qquad \text{and} \qquad \boldsymbol{x}_B^* = (\mu, 0). \tag{71}$$

The Jacobian of the system evaluated at $\boldsymbol{x}_A = (0, 0)$ is

$$\boldsymbol{J_f}(\boldsymbol{x}_B^*(\mu), \mu) = \begin{bmatrix} 0 & 1 \\ -\mu & -1 \end{bmatrix} \tag{72}$$

and it has eigenvalues (see Figure 14)

$$\lambda_{1,2}(\mu) = \frac{-1 \pm \sqrt{1 - 4\mu}}{2}. \tag{73}$$

For $\mu^* = 0$ the two fixed point are both located at $(0, 0)$ and the system has eigenvalues

$$\lambda_1(\mu^*) = -1, \qquad \lambda_2(\mu^*) = 0. \tag{74}$$

Hence for $\mu^* = 0$ the fixed point $(0, 0)$ is non-hyperbolic. The eigenvectors of $\boldsymbol{J_f}$ corresponding to $\lambda_1(\mu^*)$ and $\lambda_2(\mu^*)$ are

$$\boldsymbol{v}_1 = \begin{bmatrix} 1 \\ -1 \end{bmatrix}, \qquad \boldsymbol{v}_1 = \begin{bmatrix} 1 \\ 0 \end{bmatrix}. \tag{75}$$

To study the normal form of the system at the fixed point $(0, 0)$, we include μ as phase variable, i.e., we consider the *extended system*

$$\begin{cases} \dot{x}_1 = x_2 \\ \dot{x}_2 = -x_2 + \mu x_1 - x_1^2 \\ \dot{\mu} = 0 \end{cases} \tag{76}$$

The Jacobian at $(x_1, x_2, \mu) = (0, 0, 0)$ is

$$\boldsymbol{J_f}(0, 0, 0) = \begin{bmatrix} 0 & 1 & 0 \\ 0 & -1 & 0 \\ 0 & 0 & 0 \end{bmatrix} \tag{77}$$

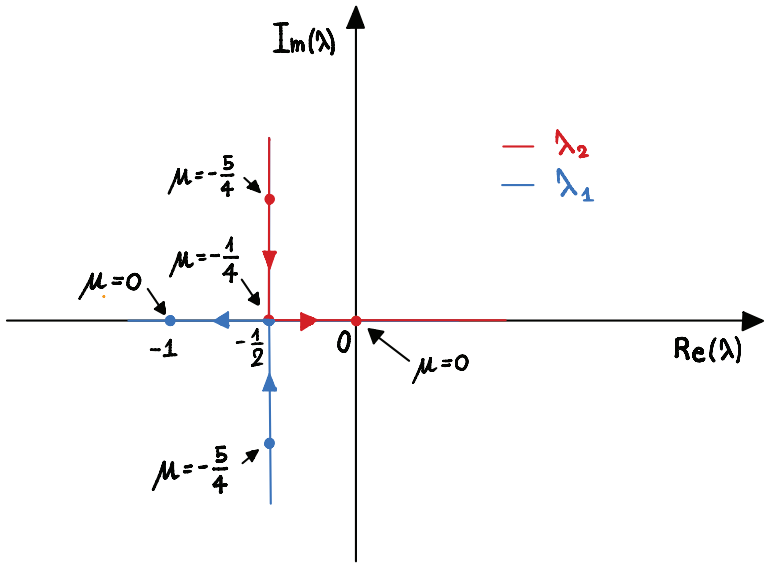

Figure 14: Eigenvalues of the Jacobian matrix (72) as a function of μ.

and it has eigenvalues

$$\lambda_1 = 0 \quad \text{(multiplicity 2)}, \qquad \lambda_2 = -1 \quad \text{(multiplicity 1)}. \tag{78}$$

Therefore the system has a two-dimensional center subspace V^c, and a one-dimensional stable subspace V^s spanned by the eigenvectors

$$V^c = \text{span}\left\{ \begin{bmatrix} 1 \\ 0 \\ 0 \end{bmatrix}, \begin{bmatrix} 0 \\ 0 \\ 1 \end{bmatrix} \right\}, \qquad V^s = \text{span}\left\{ \begin{bmatrix} 1 \\ -1 \\ 0 \end{bmatrix} \right\}. \tag{79}$$

We choose the similarity matrix $\boldsymbol{P}$ that transforms $\boldsymbol{J_f}(0,0,0)$ to a diagonal form as

$$\boldsymbol{P} = \begin{bmatrix} 1 & 1 & 0 \\ 0 & -1 & 0 \\ 0 & 0 & 1 \end{bmatrix}. \tag{80}$$

In this way we have

$$\boldsymbol{J_f}(0,0,0) = \boldsymbol{P}\boldsymbol{\Lambda}\boldsymbol{P}^{-1} \qquad \text{where} \qquad \boldsymbol{\Lambda} = \begin{bmatrix} 0 & 0 & 0 \\ 0 & -1 & 0 \\ 0 & 0 & 0 \end{bmatrix}. \tag{81}$$

That matrix factorization (81) defines the change of variables[11]

$$\begin{bmatrix} c \\ s \\ r \end{bmatrix} = \underbrace{\begin{bmatrix} 1 & 1 & 0 \\ 0 & -1 & 0 \\ 0 & 0 & 1 \end{bmatrix}}_{\boldsymbol{P}^{-1}} \begin{bmatrix} x_1 \\ x_2 \\ \mu \end{bmatrix} = \begin{bmatrix} x_1 + x_2 \\ -x_2 \\ \mu \end{bmatrix} \qquad \Leftrightarrow \qquad \begin{bmatrix} x_1 \\ x_2 \\ \mu \end{bmatrix} = \underbrace{\begin{bmatrix} 1 & 1 & 0 \\ 0 & -1 & 0 \\ 0 & 0 & 1 \end{bmatrix}}_{\boldsymbol{P}} \begin{bmatrix} c \\ s \\ r \end{bmatrix} = \begin{bmatrix} c + s \\ -s \\ r \end{bmatrix}. \tag{84}$$

[11] Recall that we can always write a nonlinear dynamical system $\dot{\boldsymbol{x}} = \boldsymbol{f}(\boldsymbol{x})$ at a fixed point $\boldsymbol{x}^*$ as

$$\begin{aligned} \dot{\boldsymbol{\eta}} &= \boldsymbol{J_f}(\boldsymbol{x}^*)\boldsymbol{\eta} + \boldsymbol{g}(\boldsymbol{\eta}) \\ &= \boldsymbol{P}\boldsymbol{\Lambda}\boldsymbol{P}^{-1}\boldsymbol{\eta} + \boldsymbol{g}(\boldsymbol{\eta}). \end{aligned} \tag{82}$$

Defining $\boldsymbol{q} = \boldsymbol{P}^{-1}\boldsymbol{\eta}$ and substituting it in the equation above yields

$$\dot{\boldsymbol{q}} = \boldsymbol{\Lambda}\boldsymbol{q} + \boldsymbol{P}^{-1}\boldsymbol{g}(\boldsymbol{P}\boldsymbol{q}). \tag{83}$$

This allows us to transform the system (70) in coordinates (c,s,r) as

$$\dot{c} = \dot{x}_1 + \dot{x}_2 = x_2 - x_2 + \mu x_1 - x_1^2 = r(c+s) - (c+s)^2, \tag{85}$$

$$\dot{s} = -\dot{x}_2 = x_2 - \mu x_1 + x_1^2 = -s - r(c+s) + (c+s)^2, \tag{86}$$

i.e.,

$$\begin{cases} \dot{c} = r(c+s) - (c+s)^2 \\ \dot{s} = -s - r(c+s) + (c+s)^2 \\ \dot{r} = 0 \end{cases} \tag{87}$$

Now we calculate the center manifold of the system (87). Such manifold must be: 1) pass through the point $(c,s,r) = (0,0,0)$, be tangent to V^c at $(c,s,r) = (0,0,0)$, be invariant under (87), 2) The vectors defining the center subspace V^c in the new coordinate system (c,s,r) are (see V^c in equation (79))

$$\underbrace{\begin{bmatrix} 1 & 1 & 0 \\ 0 & -1 & 0 \\ 0 & 0 & 1 \end{bmatrix}}_{\boldsymbol{P}^{-1}} \begin{bmatrix} 1 \\ 0 \\ 0 \end{bmatrix} = \begin{bmatrix} 1 \\ 0 \\ 0 \end{bmatrix}, \qquad \underbrace{\begin{bmatrix} 1 & 1 & 0 \\ 0 & -1 & 0 \\ 0 & 0 & 1 \end{bmatrix}}_{\boldsymbol{P}^{-1}} \begin{bmatrix} 0 \\ 0 \\ 1 \end{bmatrix} = \begin{bmatrix} 0 \\ 0 \\ 1 \end{bmatrix} \tag{88}$$

The local center manifold can be represented by the two-dimensional polynomial

$$s = h(c,r) = a_0 + a_1 c + a_2 r + a_3 c^2 + a_4 cr + a_5 r^2 + \cdots . \tag{89}$$

By definition, the center manifold passes through the fixed point $(c,s,r) = (0,0,0)$ and is tangent to

$$V^c = \text{span} \left\{ \begin{bmatrix} 1 \\ 0 \\ 0 \end{bmatrix}, \begin{bmatrix} 0 \\ 0 \\ 1 \end{bmatrix} \right\} \tag{90}$$

at $(c,s,r) = (0,0,0)$. Imposing these two conditions yields

$$h(0,0) = 0 \quad \Rightarrow \quad a_0 = 0, \qquad \nabla h(0,0) = (0,0) \quad \Rightarrow \quad a_1 = 0, \quad a_2 = 0. \tag{91}$$

Hence we are left with the expression

$$s = h(c,r) = a_3 c^2 + a_4 cr + a_5 r^2 + \cdots . \tag{92}$$

The coefficients $\{a_3, a_4, \dots, \}$ can be determined by imposing that the center manifold is an invariant manifold, i.e.,

$$\dot{s} = \frac{\partial h(c,r)}{\partial c}\dot{c} + \frac{\partial h}{\partial r}\dot{r} = \frac{\partial h}{\partial c}\dot{c} + \frac{\partial h}{\partial r}0 = \frac{\partial h}{\partial c}\dot{c}. \tag{93}$$

Substituting the equations of motion (87) into (93) yields

$$-s - r(c+s) + (c+s)^2 = (2a_3 c + a_4 r)\left(r(c+s) - (c+s)^2\right). \tag{94}$$

Now we replace s with the power series expansion (92) and we match the coefficients multiplying the same powers of c and r. This yields (after some algebra)

$$a_3 = 1, \quad a_4 = -1, \quad a_5 = 0. \tag{95}$$

Therefore the local center manifold (92) can be written as

$$s = h(c,r) = c^2 - rc + \cdots \tag{96}$$

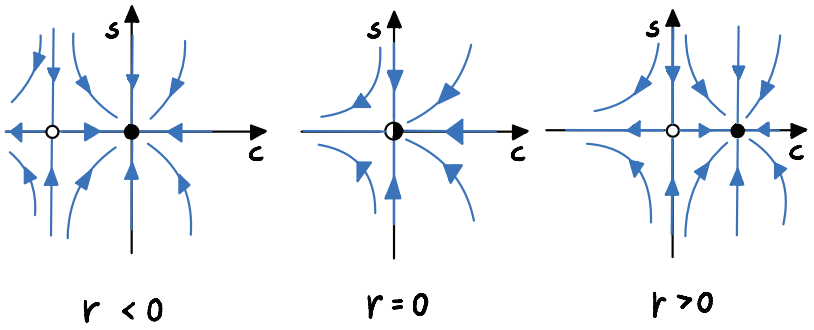

Figure 15: Sketch of the 2D transcritical bifurcation process described by the normal form (98).

Substituting this result back into (87) and assuming that c, s and r are very small yields the system

$$\begin{cases} \dot{c} = r(c + c^2 - rc) - (c + c^2 - rc)^2 \simeq rc - c^2 \\ \dot{s} = -s - r(c + s) + (c + s)^2 \simeq -s \\ \dot{r} = 0 \end{cases} \tag{97}$$

Hence, in a neighborhood of the the fixed point $(c, s, r) = (0, 0, 0)$, the system (87) can be written as

$$\begin{cases} \dot{c} = rc - c^2 \\ \dot{s} = -s \end{cases} \tag{98}$$

This is the normal form of a transcritical bifurcation in two dimensions. The phase portraits of (98) for different r are sketched in Figure 15.

Saddle-node bifurcation. Consider the two dimensional system

$$\begin{cases} \dot{x}_1 = x_2 \\ \dot{x}_2 = x_2 - x_1^2 - \mu \end{cases} \tag{99}$$

For $\mu < 0$ the system has two fixed points located at

$$\boldsymbol{x}^*_{A,B} = (\pm\sqrt{-\mu}, 0). \tag{100}$$

Clearly, for $\mu = 0$ these two points coincide and they both disappear for $\mu > 0$ (see Figure 16). So, it seems that the system is undergoes a saddle-node bifurcation. Let us verify analytically that this is indeed the case. The Jacobian of the system evaluated at the fixed point $(x_1^*, x_2^*, \mu^*) = (0, 0, 0)$ is

$$\boldsymbol{J_f}(0, 0, 0) = \begin{bmatrix} 0 & 1 \\ 0 & 1 \end{bmatrix} \tag{101}$$

and it has eigenvalues (see Figure 14)

$$\lambda_1 = 0, \qquad \lambda_2 = 1. \tag{102}$$

the corresponding eigenvectors are

$$\boldsymbol{v}_1 = \begin{bmatrix} 1 \\ 0 \end{bmatrix}, \qquad \boldsymbol{v}_2 = \begin{bmatrix} 1 \\ 1 \end{bmatrix}. \tag{103}$$

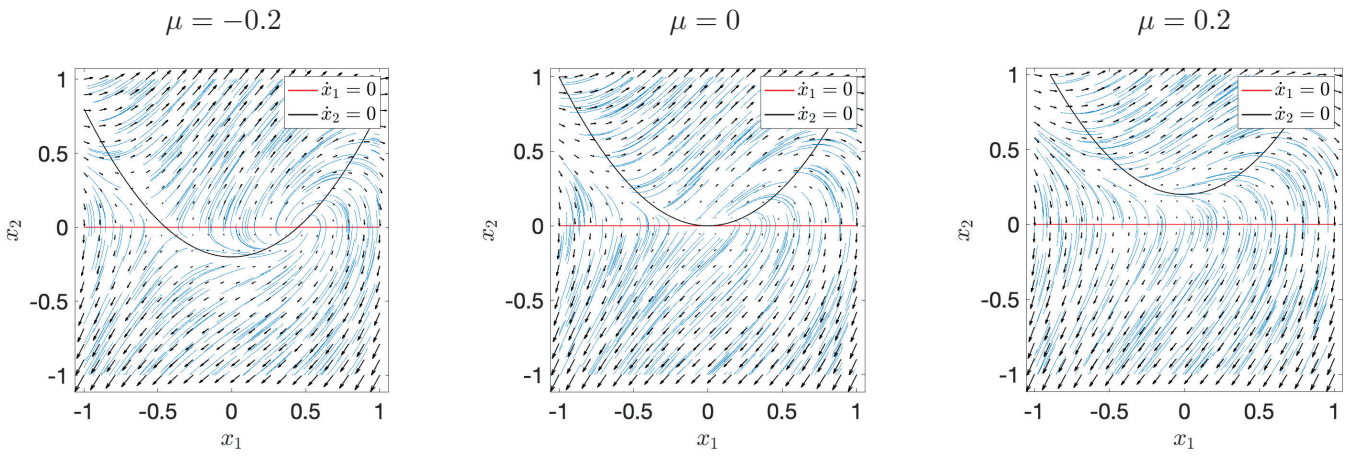

Figure 16: Phase portraits of the system (99) for different μ. Note that the system seems to have a spiral before and after the bifurcation, but actually when μ approaches zero such spiral becomes a stable node as predicted by the normal form (123). Note also that since the bifurcation is local the *index* is preserved before and after bifurcation. Therefore, the index of the non-hyperbolic fixed point at $(x_1^*, x_2^*, \mu^*) = (0, 0, 0)$ is zero (saddle node + repellor).

To compute the normal form of the system at the bifurcation point (Jacobian non-invertible) we consider the extended system

$$\begin{cases} \dot{x}_1 = x_2 \\ \dot{x}_2 = x_2 - x_1^2 - \mu \\ \dot{\mu} = 0 \end{cases} \tag{104}$$

The Jacobian of the extended system (104) at $(x_1, x_2, \mu) = (0, 0, 0)$ is

$$\boldsymbol{J_f}(0,0,0) \begin{bmatrix} 0 & 1 & 0 \\ 0 & 1 & -1 \\ 0 & 0 & 0 \end{bmatrix} \tag{105}$$

and has eigenvalues

$$\lambda_1 = 0 \quad \text{(multiplicity 2)}, \qquad \lambda_2 = 1 \quad \text{(multiplicity 1)}. \tag{106}$$

In this case the eigenvalue $\lambda_1 = 0$ has geometric multiplicity one and therefore the center subspace V^c is spanned by

$$V^c = \text{span} \left\{ \begin{bmatrix} 1 \\ 0 \\ 0 \end{bmatrix} \quad \text{(eigenvector)}, \begin{bmatrix} 0 \\ 1 \\ 1 \end{bmatrix} \quad \text{(generalized eigenvector)} \right\}. \tag{107}$$

The unstable subspace V^u is spanned by the eigenvector

$$V^u = \text{span} \left\{ \begin{bmatrix} 1 \\ 1 \\ 0 \end{bmatrix} \right\}. \tag{108}$$

We consider the similarity transformation

$$\boldsymbol{P} = \begin{bmatrix} 1 & 1 & 0 \\ 0 & 1 & 1 \\ 0 & 0 & 1 \end{bmatrix} \tag{109}$$

$\boldsymbol{P}$ transform $\boldsymbol{J_f}(0,0,0)$ into the Jordan form

$$\boldsymbol{K} = \begin{bmatrix} 0 & 0 & 1 \\ 0 & 1 & 0 \\ 0 & 0 & 0 \end{bmatrix} \qquad \text{via} \qquad \boldsymbol{J_f}(0,0,0) = \boldsymbol{P}\boldsymbol{K}\boldsymbol{P}^{-1}. \tag{110}$$

The transformation $\boldsymbol{P}$ also defines the coordinate change

$$\begin{bmatrix} c \\ u \\ r \end{bmatrix} = \underbrace{\begin{bmatrix} 1 & -1 & 1 \\ 0 & 1 & -1 \\ 0 & 0 & 1 \end{bmatrix}}_{\boldsymbol{P}^{-1}} \begin{bmatrix} x_1 \\ x_2 \\ \mu \end{bmatrix} = \begin{bmatrix} x_1 - x_2 + \mu \\ x_2 - \mu \\ \mu \end{bmatrix} \qquad \Leftrightarrow \qquad \begin{bmatrix} x_1 \\ x_2 \\ \mu \end{bmatrix} = \underbrace{\begin{bmatrix} 1 & 1 & 0 \\ 0 & 1 & 1 \\ 0 & 0 & 1 \end{bmatrix}}_{\boldsymbol{P}} \begin{bmatrix} c \\ u \\ r \end{bmatrix} = \begin{bmatrix} c+u \\ u+r \\ r \end{bmatrix}. \tag{111}$$

The center subspace and the unstable subspace can be written in coordinates (c,u,r) as[12]

$$V^c = \text{span}\left\{ \begin{bmatrix} 1 \\ 0 \\ 0 \end{bmatrix}, \begin{bmatrix} 0 \\ 0 \\ 1 \end{bmatrix} \right\}, \qquad V^u = \text{span}\left\{ \begin{bmatrix} 0 \\ 1 \\ 0 \end{bmatrix} \right\}. \tag{113}$$

Similarly, the system (99) can be written in coordinates (c,u,r) using the mapping (111) as

$$\dot{c} = \dot{x}_1 - \dot{x}_2 + \dot{\mu} = x_2 - x_2 + x_1^2 + \mu = x_1^2 + \mu = (c+u)^2 + r, \tag{114}$$

$$\dot{u} = \dot{x}_2 - \dot{\mu} = x_2 - x_1^2 - \mu = (u+r) - (c+u)^2 - r = u - (c+u)^2. \tag{115}$$

This yields the following extended system in coordinates (c,u,r)

$$\begin{cases} \dot{c} = (c+u)^2 + r \\ \dot{u} = u - (c+u)^2 \\ \dot{r} = 0 \end{cases} \tag{116}$$

This system is completely equivalent to (104). Next, we calculate the center manifold $u = h(c,r)$ at $(c,u,r) = (0,0,0)$. As before, such center manifold must pass through $(c,u,r) = (0,0,0)$, be tangent to V^c in (113), and be invariant under (116). This immediately implies that the polynomial expansion of the local center manifold is

$$u = h(c,r) = a_1 c^2 + a_2 cr + a_3 r^2 + \cdots. \tag{117}$$

By imposing that the center manifold is invariant manifold we obtain

$$\dot{u} = \frac{\partial h}{\partial c}\dot{c} + \underbrace{\frac{\partial h}{\partial r}}_{\dot{r}=0}\dot{r} = \frac{\partial h}{\partial c}\dot{c}. \tag{118}$$

Substituting (116) and (117) into (118) yields

$$u - (c + h(c,r))^2 = (2a_1 c + a_2 r + \cdots)\left((c + h(c,r))^2 + r\right), \tag{119}$$

[12]Note that

$$\underbrace{\begin{bmatrix} 1 & -1 & 1 \\ 0 & 1 & -1 \\ 0 & 0 & 1 \end{bmatrix}}_{\boldsymbol{P}^{-1}} \underbrace{\begin{bmatrix} 1 \\ 0 \\ 0 \end{bmatrix}}_{\in V^c} = \begin{bmatrix} 1 \\ 0 \\ 0 \end{bmatrix}, \qquad \underbrace{\begin{bmatrix} 1 & -1 & 1 \\ 0 & 1 & -1 \\ 0 & 0 & 1 \end{bmatrix}}_{\boldsymbol{P}^{-1}} \underbrace{\begin{bmatrix} 0 \\ 1 \\ 1 \end{bmatrix}}_{\in V^c} = \begin{bmatrix} 0 \\ 0 \\ 1 \end{bmatrix}, \qquad \underbrace{\begin{bmatrix} 1 & -1 & 1 \\ 0 & 1 & -1 \\ 0 & 0 & 1 \end{bmatrix}}_{\boldsymbol{P}^{-1}} \underbrace{\begin{bmatrix} 1 \\ 1 \\ 0 \end{bmatrix}}_{\in V^u} = \begin{bmatrix} 0 \\ 1 \\ 0 \end{bmatrix}. \tag{112}$$

i.e.,

$$\begin{aligned}\left(a_1c^2+a_2cr+a_3r^2+\cdots\right)-\left[c+\left(a_1c^2+a_2cr+a_3r^2+\cdots\right)\right]^2=\\ \left(2a_1c+a_2r+\cdots\right)\left[\left(c+\left(a_1c^2+a_2cr+a_3r^2+\cdots\right)\right)^2+r\right].\end{aligned} \tag{120}$$

By matching the coefficients multiplying the same powers in the previous equation we obtain (after quite a bit of algebra)

$$a_1=1,\quad a_2=2,\quad a_3=2. \tag{121}$$

Hence, the local center manifold is

$$u=h(c,r)=c^2+2rc+2r^2+\cdots \tag{122}$$

Substituting this manifold into (116) and assuming that c, u and r are very small yields

$$\begin{cases}\dot{c}=c^2+r\\ \dot{u}=u\end{cases} \tag{123}$$

which is the normal form of a saddle node bifurcation in two dimensions.

Appendix B: Hopf bifurcation in Cartesian coordinates

Any trajectory $(c_1(t),c_(t))$ in a Cartesian plane (c_1,c_2). can be equivalently expressed in polar coordinates $(R(t),\vartheta(t))$ and vice versa via the well-known transformation

$$\begin{cases}c_1(t)=R(t)\cos(\vartheta(t))\\ c_2(t)=R(t)\sin(\vartheta(t))\end{cases}\quad\Leftrightarrow\quad\begin{cases}R^2(t)=c_1^2(t)+c_2^2(t)\\ \tan(\vartheta(t))=\dfrac{c_2(t)}{c_1(t)}\end{cases} \tag{124}$$

Differentiate these formulas with respect to time

$$\begin{cases}\dot{c}_1=\dot{R}\cos(\vartheta)-R\sin(\vartheta)\dot{\vartheta}=\dfrac{\dot{R}}{R}c_1-c_2\dot{\vartheta}\\ \dot{c}_2=\dot{R}\sin(\vartheta)+R\cos(\vartheta)\dot{\vartheta}=\dfrac{\dot{R}}{R}c_2+c_1\dot{\vartheta}\end{cases} \tag{125}$$

and substitute the expressions for $\dot{R}$ and $\dot{\vartheta}$ appearing in (36) to obtain

$$\begin{cases}\dot{c}_1=\dfrac{rDR+AR^3}{r}c_1-c_2(\omega+CH+BR^2)=(rD+AR^2)c_1-c_2(\omega+rC+BR^2),\\ \dot{c}_2=\dfrac{rDR+AR^3}{R}c_2+c_1(\omega+rC+BR^2)=(rD+AR^2)c_2+c_1(\omega+rC+BR^2).\end{cases} \tag{126}$$

Recalling that $R^2=c_1^2+c_2^2$ these expression can be written as

$$\begin{cases}\dot{c}_1=\left[rD+A(c_1^2+c_2^2)\right]c_1-c_2\left[\omega+rC+B(c_1^2+c_2^2)\right],\\ \dot{c}_2=\left[rD+A(c_1^2+c_2^2)\right]c_2+c_1\left[\omega+rC+B(c_1^2+c_2^2)\right],\end{cases} \tag{127}$$

which coincide with (38).

Lorenz equations

In 1963 Ed Lorenz published a paper titled *"Deterministic non-periodic flows"* in the Journal of Atmospheric Sciences in which he studied an idealization of a hydrodynamical system represented by a fluid layer between two free surfaces. The system is sketched in Figure 1.

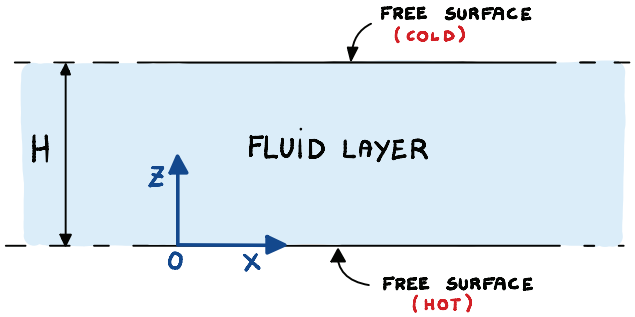

Figure 1: Fluid layer between two free surfaces. The "free surface" boundary conditions are defined by setting vertical component of the fluid velocity v_z equal zero at $z = 0$ and $z = H$ (Dirichlet boundary conditions), and the derivative of the horizontal component with respect to the vertical axis $\partial v_x/\partial z$ equal to zero at $z = 0$ and $z = H$ (Neumann boundary conditions). The free surfaces are kept at constant temperature T_{hot} (bottom surface) and $T_{\text{cold}} \leq T_{\text{hot}}$ (top surface).

The equations of motion for this system are[1]

$$\begin{cases} \dfrac{\partial \nabla^2 \Psi}{\partial t} + \dfrac{\partial \Psi}{\partial z}\dfrac{\partial}{\partial x}\nabla^2\Psi - \dfrac{\partial \Psi}{\partial x}\dfrac{\partial}{\partial z}\nabla^2\Psi = \nu\nabla^4\Psi + g\beta\dfrac{\partial \theta}{\partial x}, \\ \dfrac{\partial \theta}{\partial t} + \dfrac{\partial \Psi}{\partial z}\dfrac{\partial \theta}{\partial x} - \dfrac{\partial \Psi}{\partial x}\dfrac{\partial \theta}{\partial z} = \kappa\nabla^2\theta + \dfrac{\Delta T}{H}\dfrac{\partial \Psi}{\partial x}, \end{cases} \tag{1}$$

where $\Psi(x, z, t)$ is the streamfunction that defines the fluid velocity components as

$$v_x(x, z, t) = \frac{\partial \Psi(x, z, t)}{\partial z}, \qquad v_z(x, z, t) = -\frac{\partial \Psi(x, z, t)}{\partial x}, \tag{2}$$

$\theta(x, z, t)$ represents the deviation of the temperature distribution in the fluid layer from the pure thermal conduction state, i.e.,

$$\theta(x, z, t) = T(x, z, t) - \left(\frac{\Delta T}{H} z\right), \tag{3}$$

$\Delta T = T_{\text{hot}} - T_{\text{cold}}$ is the temperature difference between the isothermal horizonal fluid layers at $z = 0$ (hot) and $z = H$ (cold), H is the depth of the fluid layer, and g, β, ν and κ are, respectively, the acceleration of gravity, the isobaric compressibility, the kinematic viscosity, and the thermal diffusivity of the fluid. When studying natural convection problems it is convenient to define the following dimensionless number

$$Ra = \frac{g\beta H^3 \Delta T}{\nu\kappa} \qquad \text{(Rayleigh number)} \tag{4}$$

which represents the relative importance between the effects of the buoyancy forces due to temperature differences, and the effects of the viscosity forces.

[1]The model equations (1) are called Oberbeck-Boussinesq approximation of the natural convection problem. The first equation in (1) is the Navier-Stokes equation written in a 2D streamfunction-vorticity formulation. The second equation is the Fourier equation governing the the propagation of temperature within the fluid layer due to diffusion and transport by the fluid velocity.

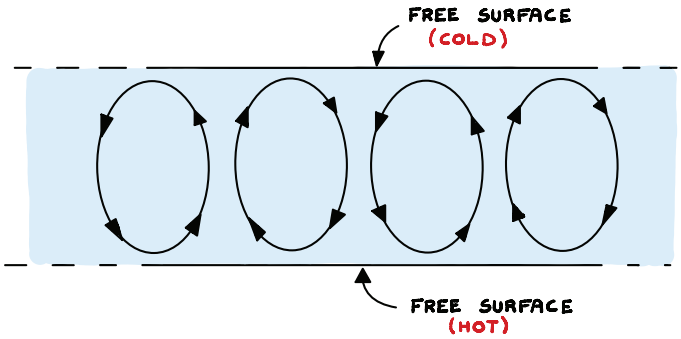

Figure 2: One-roll convection patterns arising in the infinite fluid layer system sketched in Figure 1. The convection patter is generated for Rayleigh numbers Ra slightly above the critical one $Ra_c = 657.5$ (onset of convective instability).

Intuitively, when the buoyancy forces exceed some threshold depending on thermal diffusivity and viscosity the fluid then the system transitions from a state of pure thermal conduction to natural convection, with an infinite number of one-roll patterns as shown in Figure 2. The critical Rayleigh number that characterizes the transition point between thermal condition and natural convection is called *onset of convective instability*. For the system sketched in Figure 1 the critical Rayleigh number can be computed analytically as

$$Ra_c = \frac{27\pi^4}{4} = 657.5. \tag{5}$$

For $Ra < Ra_c$ the fluid does not move, while for Ra slightly above Ra_c we have an infinite number of one-roll convection patterns (see Figure 2). The system transitions from the no-flow state to the one-roll convection pattern state via a *supercritical pitchfork bifurcation*. By expanding θ and Ψ in (1) in a double Fourier series as and projecting onto the Fourier basis it is possible to transform (1) into a finite-dimensional nonlinear system of differential equations for the time-dependent functions (Fourier coefficients) representing the coefficients of the expansion.

In certain cases, all except three Fourier coefficients eventually tend to zero, and those three modes undergo irregular non-periodic fluctuations. Lorenz observed that the same solutions would have been obtained if the Fourier series had at the start been truncated to include a total number of three terms. Accordingly, he looked for time-dependent solutions of (1) in the form

$$\Psi(x,z,t) = 3\kappa X(t) \sin\left(\frac{\pi}{\sqrt{2}H}x\right)\sin\left(\frac{\pi}{H}z\right), \tag{6}$$

$$\theta(x,z,t) = \frac{\Delta T Ra_c}{\pi Ra}\left[\sqrt{2}Y(t)\cos\left(\frac{\pi}{\sqrt{2}H}x\right)\sin\left(\frac{\pi}{H}z\right) - Z(t)\sin\left(\frac{2\pi}{H}z\right)\right], \tag{7}$$

where $X(t)$, $Y(t)$ and $Z(t)$ are the Fourier coefficients (functions of time alone). By substituting (6)-(7) into (1) and omitting trigonometric terms other that those occurring in (6)-(7) we obtain

$$\begin{cases} \dot{X} = -\sigma X + \sigma Y \\ \dot{Y} = rX - Y - XZ \qquad \text{(Lorenz system)} \\ \dot{Z} = XY - bZ \end{cases} \tag{8}$$

In ODE system above, the time derivative is with respect to the dimensionless time

$$\tau = \frac{3\pi^2\kappa}{2H^2}t, \tag{9}$$

and the parameters r, σ and b are defined as

$$\begin{cases} r = \dfrac{Ra}{Ra_c} & \text{(relative Rayleigh number)} \\ \sigma = \dfrac{\nu}{\kappa} & \text{(Prandtl number)} \\ b = \dfrac{8}{3} \end{cases} \tag{10}$$

The system of equations (6)-(8) represents a simplified solution to the natural convection equations (1). In fact, with $X(t)$, $Y(t)$ and $Z(t)$ available from (8) we can then reconstruct the velocity and temperature fields within the fluid layer by using (6) and(7).

Properties of the Lorenz system. The Lorenz system is a three-dimensional nonlinear dynamical system with quadratic polynomial non-linearities. Additionally, it possesses the following fundamental properties.

- **Symmetry.** The transformation $(X, Y) \to (-X, -Y)$ leaves the system (8) invariant. This implies that the phase portrait is symmetric with respect to the Z-axis. As a consequence, trajectories with initial condition on Z-axis stay on the Z-axis for all times. This can be also seen by noting that the initial condition $(0, 0, Z_0)$ yields a trajectory described by the system $\dot{X} = 0$, $\dot{Y} = 0$, $\dot{Z} = -bZ$.

- **Volume contraction.** The volume of any compact region $D(t) \subset \mathbb{R}^3$ advected by the flow of any three dimensional system evolves in time as (see Theorem 2 in Appendix A)

$$\frac{dV(t)}{dt} = \int_{D(t)} \nabla \cdot \boldsymbol{f}(\boldsymbol{x}) d\boldsymbol{x}. \tag{11}$$

  The divergence of vector field at the right hand side of the Lorenz system (8) is

$$\begin{aligned} \nabla \cdot \boldsymbol{f} =& \frac{\partial f_1}{\partial X} + \frac{\partial f_2}{\partial Y} + \frac{\partial f_3}{\partial Z} \\ =& \frac{\partial}{\partial X}(-\sigma X + \sigma Y) + \frac{\partial}{\partial Y}(rX - Y - XZ) + \frac{\partial}{\partial Z}(XY - bZ) \\ =& -(\sigma + b + 1). \end{aligned} \tag{12}$$

  Recalling that σ and b are positive numbers we see that $\nabla \cdot \boldsymbol{f} < 0$ at each point in phase space. By substituting (12) into (11) we obtain

$$\frac{dV(t)}{dt} = -(\sigma + b + 1) \int_{D(t)} 1 d\boldsymbol{x} = -(\sigma + b + 1) V(t), \tag{13}$$

  i.e

$$V(t) = V(0) e^{-(\sigma + b + 1)t}. \tag{14}$$

  Hence, the volume of *any* compact region advected by the flow generated by (8) shrinks to zero exponentially fast in time, independently of where we pick the region, or its initial shape.

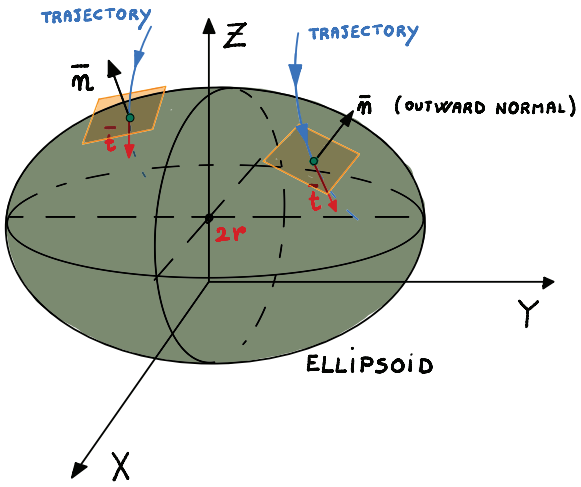

Figure 3: Trajectories of the Lorenz system do not escape the ellipsoid (15) if Q is chosen large enough.

- **Trajectories are bounded.** Consider the ellipsoid

$$E(Q) = \{(x, y, z) \in \mathbb{R}^3 : rx^2 + \sigma y^2 + \sigma(z - 2r)^2 = Q\}, \tag{15}$$

where Q is a positive number representing how big the ellipsoid is[2]. The outward normal to the surface of the ellipsoid is (see Figure 3)

$$\boldsymbol{n} = (2rx, 2\sigma y, 2\sigma(z - 2r)) \tag{18}$$

and it coincides with the components of the gradient of

$$F(x, y, z) = rx^2 + \sigma y^2 + \sigma(z - 2r) - Q \tag{19}$$

evaluated at the zero level set of F. The tangent vector to an arbitrary trajectory intersecting the surface of the ellipsoid (15) at a point $(x_e, y_e, z_e) \in E(Q)$ is given by the right hand side of (8) evaluated at (x_e, y_e, z_e), i.e.,

$$\boldsymbol{t} = (-\sigma x_e + \sigma y_e, rx_e - y_e - x_e z_e, x_e y_e - b z_e)\,. \tag{20}$$

Taking the dot product between the outward normal vector (18) and the vector tangent to a trajectory passing through an arbitrary point on the ellipsoid (15) yields

$$\begin{aligned} \boldsymbol{n} \cdot \boldsymbol{t} =& 2rx_e(-\sigma x_e + \sigma y_e) + 2\sigma y_e(rx_e - y_e - x_e z_e) + 2\sigma(z_e - 2r)(x_e y_e - b z_e) \\ =& -2\sigma \left(rx_e^2 + y_e^2 + b(z_e - r)^2 - br^2\right). \end{aligned} \tag{21}$$

Clearly, if

$$rx_e^2 + y_e^2 + b(z_e - r)^2 > br^2, \tag{22}$$

[2]Note that the ellipsoid (15) is centered at $(x, y, z) = (0, 0, 2r)$ and it can be written as

$$\frac{x^2}{Q/r} + \frac{y^2}{Q/\sigma} + \frac{(z - 2r)^2}{Q/\sigma} = 1. \tag{16}$$

In this form we see that the semi-axes are

$$a_1 = \sqrt{\frac{Q}{r}}, \qquad a_2 = \sqrt{\frac{Q}{\sigma}}, \qquad a_3 = \sqrt{\frac{Q}{\sigma}}. \tag{17}$$

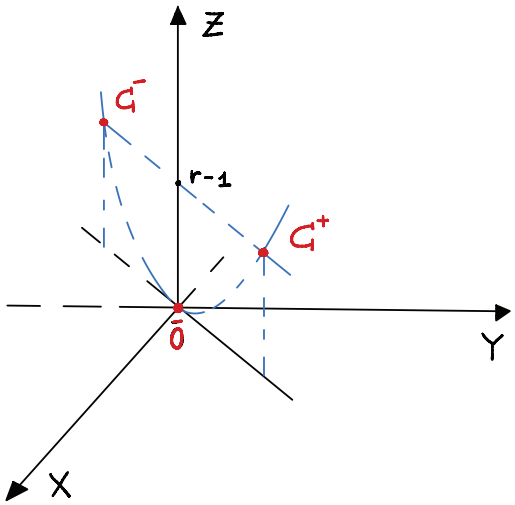

Figure 4: Fixed points of the Lorenz system for $r > 1$.

then $\boldsymbol{n} \cdot \boldsymbol{t} < 0$, i.e., the vector tangent to the trajectory intersecting the surface of the ellipsoid points inward. Of course, if Q in (15) is sufficiently large, then all points on the surface of the ellipsoid $E(Q)$ will satisfy condition (22). This proves that the ellipsoid itself will serve as the boundary for the trajectories corresponding to any initial condition on its surface or inside it.

Stability analysis of fixed points. The nullclines of (8) are

$$\begin{cases} X = Y \\ Y = rX - XZ \\ Z = \dfrac{XY}{b} \end{cases} \tag{23}$$

Substituting last equation into the second and taking the first into account yields

$$X - rX + \frac{X^3}{b} = 0 \quad \Rightarrow \quad X\left(1 - r + \frac{X^2}{b}\right) = 0 \quad \Rightarrow \quad \begin{cases} X^* = 0 \\ X^* = \pm\sqrt{b(r-1)} \end{cases} \tag{24}$$

By Substituting this back into (23) we obtain the following three fixed points:

$$(0,0,0) \qquad \text{for all } r \tag{25}$$

and

$$\boldsymbol{C}^{\pm} = \left(\pm\sqrt{b(r-1)}, \pm\sqrt{b(r-1)}, r-1\right) \qquad \text{for } r > 1. \tag{26}$$

These fixed points shown in Figure 4 for $r > 1$. The stability of the fixed points is determined by the eigenvalues of the Jacobian matrix

$$\boldsymbol{J_f}(X,Y,Z) = \begin{bmatrix} -\sigma & \sigma & 0 \\ r - Z & -1 & -X \\ Y & X & -b \end{bmatrix} \tag{27}$$

evaluated at $(X^*, Y^*, Z^*) = (0,0,0)$ and $(X^*, Y^*, Z^*) = \boldsymbol{C}^{\pm}$.

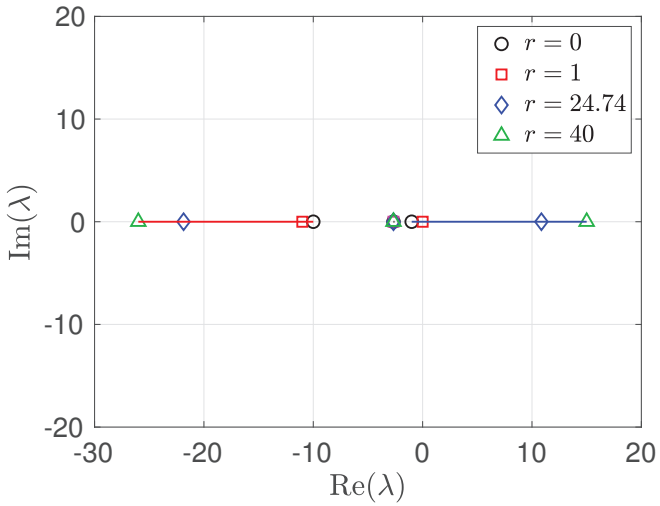

Figure 5: Stability analysis of the origin. Shown are eigenvalues of the Jacobian matrix (28) as a function of r for $b = 8/3$ and $\sigma = 10$. The origin undergoes a zero-eigenvalue bifurcation (supercritical pitchfork) for $r = 1$.

- **Stability analysis of the origin.** Evaluating the Jacobian (27) at $(X^*, Y^*, Z^*) = (0, 0, 0)$ yields

$$\boldsymbol{J_f}(0,0,0) = \begin{bmatrix} -\sigma & \sigma & 0 \\ r & -1 & 0 \\ 0 & 0 & -b \end{bmatrix} \tag{28}$$

The eigenvalues are the roots of the third-order characteristic polynomial

$$p(\lambda) = \det\left(\boldsymbol{J_f} - \lambda \boldsymbol{I}\right) = -(b+\lambda)\left[(\sigma+\lambda)(1+\lambda) - r\sigma\right], \tag{29}$$

i.e.,

$$\lambda_{1,2} = \frac{-(\sigma+1) \pm \sqrt{(\sigma+1)^2 - 4\sigma(1-r)}}{2}, \qquad \lambda_3 = -b. \tag{30}$$

It is easy to show that all eigenvalues are real[3] for each r (see Figure 5).

Specifically,

a) For $r < 1$ we have that $\lambda_{1,2,3} < 0$, i.e., the origin is a stable node. Such stable node is *globally attracting*, i.e., it attracts all trajectories disregarding where the initial condition is.

b) For $r = 1$ we have that $\lambda_{2,3} < 0$, and $\lambda_1 = 0$, i.e., the origin is a non-hyperbolic fixed point. For $r = 1$ the Jacobian (28) has one zero eigenvalue, i.e., the system undergoes a *zero-eigenvalue bifurcation*. Using Sotomayor's Theorem 6 in course note 9, it can be shown that such bifurcation is a *supercritical pitchfork bifurcation* representing the onset of convective instability of the fluid layer (note that for $r = 1$ we have $Ra = Ra_c$ in (10)). Such bifurcation generates three fixed point for $r \geq 1$, i.e., the origin (which becomes a 3D saddle node) and two stable nodes $\boldsymbol{C}^{\pm}$.

c) For $r > 1$ we have that $\lambda_{2,3} < 0$, and $\lambda_1 > 0$, i.e., the origin is a three-dimensional saddle node with two stable manifolds and one unstable manifold. The eigenvectors corresponding to $\lambda_1 < 0$ and $\lambda_2 > 0$ lie in the (X, Y)-plane, while the eigenvector corresponding to $\lambda_3 = -b < 0$ lies on the Z-axis.

[3]Note that the smallest value of the quantity within the square root in $\lambda_{1,2}$ defined in (30) is positive. In fact, such value is achieved for $r = 0$ and can be written as

$$(\sigma+1)^2 - 4\sigma = (\sigma-1)^2 > 0. \tag{31}$$

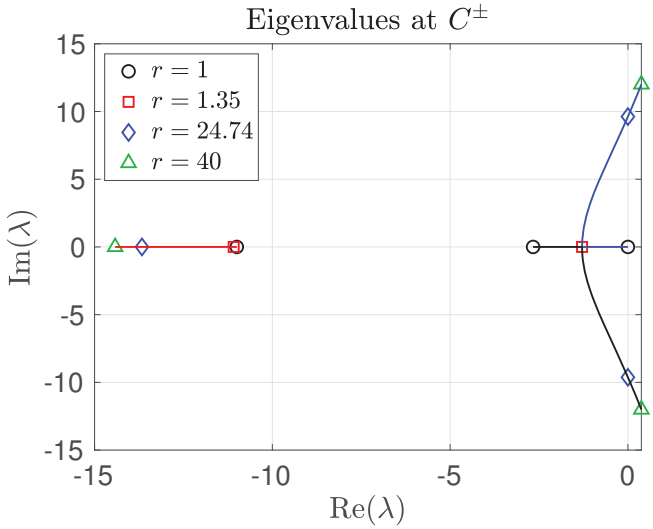

Figure 6: Stability analysis of $\boldsymbol{C}^{\pm}$. Shown are eigenvalues of the Jacobian matrix (32) as a function of r for $b = 8/3$ and $\sigma = 10$. The fixed points $\boldsymbol{C}^{\pm}$ undergo a *subcritical Hopf* bifurcation for $r = 24.74$.

- **Stability analysis of $\boldsymbol{C}^{\pm}$.** Evaluating the Jacobian (27) at $(X^*, Y^*, Z^*) = \boldsymbol{C}^{\pm}$ yields

$$\boldsymbol{J_f}\left(\boldsymbol{C}^{\pm}\right) = \begin{bmatrix} -\sigma & \sigma & 0 \\ 1 & -1 & \mp\sqrt{b(r-1)} \\ \pm\sqrt{b(r-1)} & \pm\sqrt{b(r-1)} & -b \end{bmatrix} \tag{32}$$

The eigenvalues of $\boldsymbol{J_f}(\boldsymbol{C}^{\pm})$ are roots of the characteristic polynomial

$$p(\lambda) = \det\left(\boldsymbol{J_f} - \lambda \boldsymbol{I}\right) = -(\sigma+\lambda)\left[(1+\lambda)(b+\lambda) + b(r-1)\right] + \sigma\left[(b+\lambda) - b(r-1)\right], \tag{33}$$

i.e.,

$$\lambda^3 + (\sigma + b + 1)\lambda^2 + (r+\sigma)b\lambda + 2b\sigma(r-1) = 0. \tag{34}$$

In Figure 6 we plot the eigenvalues of (32), i.e., the roots of (34), as a function of r. We see that

a) For $1 < r \leq 1.35$ the fixed points $C^{\pm}$ are stable nodes.

b) For $1.35 < r < 24.74$ the fixed points $C^{\pm}$ are still stable but there exist two complex conjugate eigenvalues with negative real part. The real Jordan form of (32) allow us to identify a plane on which the local dynamics around $\boldsymbol{C}^{\pm}$ is equivalent to a stable spiral (see Figure 7 in the course note 4).

c) For $r = 24.74$ both fixed points $C^{\pm}$ undergo a *subcritical Hopf bifurcation*. To identify the value of r at which such Hopf bifurcation occurs we set $\lambda = \omega i$ in (34), i.e.,

$$-i\omega^3 - (\sigma + b + 1)\omega^2 + i(r+\sigma)b\omega + 2b\sigma(r-1) = 0. \tag{35}$$

In other words, we look for the value of r that yields an imaginary eigenvalue. Setting the real and the imaginary parts of the complex number at the left hand side of (35) equal to zero yields, respectively,

$$\omega^2 = \frac{2b\sigma(r-1)}{\sigma + b + 1}, \qquad \omega^2 = (r+\sigma)b. \tag{36}$$

By substituting ω^2 from one equation into the other we obtain

$$r_H = \sigma\frac{\sigma + b + 3}{\sigma - (b+1)}. \tag{37}$$

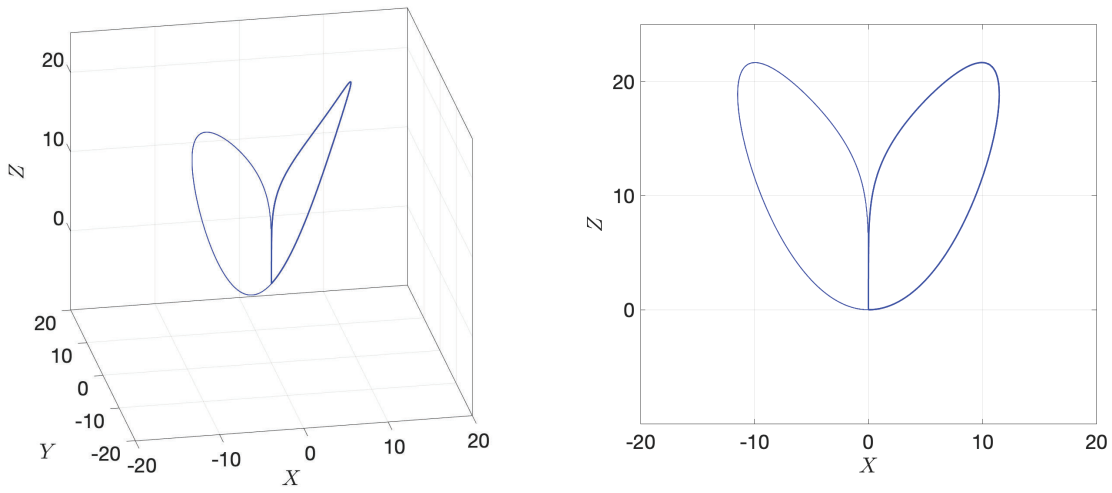

Figure 7: Homoclinic butterfly for $r = 13.92655741$, $\sigma = 10$ and $b = 8/3$. For $r > 13.92655741$ a complicated set is created at the origin of the system via a process called "homoclinic explosion". This process is described, e.g., in the book *"The Lorenz Equations: Bifurcations, Chaos,and Strange Attractors"*, by Colin Sparrow (Springer 1984). The set arising form the homoclinic explosion can yield *transient chaos* (see Figure 8).

This is the critical value of the relative Rayleigh number r at which the subcritical Hopf bifurcation occurs. For $\sigma = 10$ and $b = 8/3$ (37) yields $r_H = 24.74$ (see Figure 6).

d) For $r > 24.74$ the fixed points $\boldsymbol{C}^{\pm}$ are unstable spirals in 3D, with a stable manifold of dimension 1 (we have a one-dimensional eigenspace corresponding to a negative eigenvalue).

Summary of the bifurcation analysis of equilibria. Let us provide a brief summary of our findings related to the stability analysis of the fixed points as a function of the relative Rayleigh number r.

- For $r < 1$ there is only one fixed point at the origin (stable node) and it is globally attracting.
- For $r = 1$ the origin is non-hyperbolic (but still a stable node). The origin undergoes a supercritical pitchfork bifurcation, which yields two new fixed points $\boldsymbol{C}^{\pm}$.
- For $1 < r < r_H$ the origin is unstable (3D saddle node with a one-dimensional unstable manifold) while $\boldsymbol{C}^{\pm}$ turn from stable nodes to 3D stable spirals. Such transition happens at $r = 1.35$ for $\sigma = 10$ and $b = 8/3$. As r approaches r_H from the left, two unstable limit cycles approach the stable spirals at $\boldsymbol{C}^{\pm}$.
- For $r = r_H$ both fixed points $\boldsymbol{C}^{\pm}$ undergo a subcritical Hopf bifurcation in which the unstable cycles mentioned above are created and exist for $r < r_H$. As we reduce r below r_H, the two unstable cycles become bigger and bigger and they eventually end up touching each other at the origin for $r^* = 13.92655741$, creating the so-called *homoclinc butterfly* shown in Figure 7. For $r > r^*$ a complicated set is created at the origin via a bifurcation process called "homoclinic explosion". This process is described, e.g., in the book *"The Lorenz Equations: Bifurcations, Chaos, and Strange Attractors"*, by Colin Sparrow (Springer 1984). The set arising form the homoclinic explosion can yield *transient chaotic trajectories*, as shown in Figure 8.
- For $r > r_H$ the fixed points $\boldsymbol{C}^{\pm}$ are both three-dimensional unstable spirals. Both spirals have a one-dimensional stable manifold.

Hence, for $r > r_H$ there are no stable fixed points as both the origin and $\boldsymbol{C}^{\pm}$ are unstable. However, we

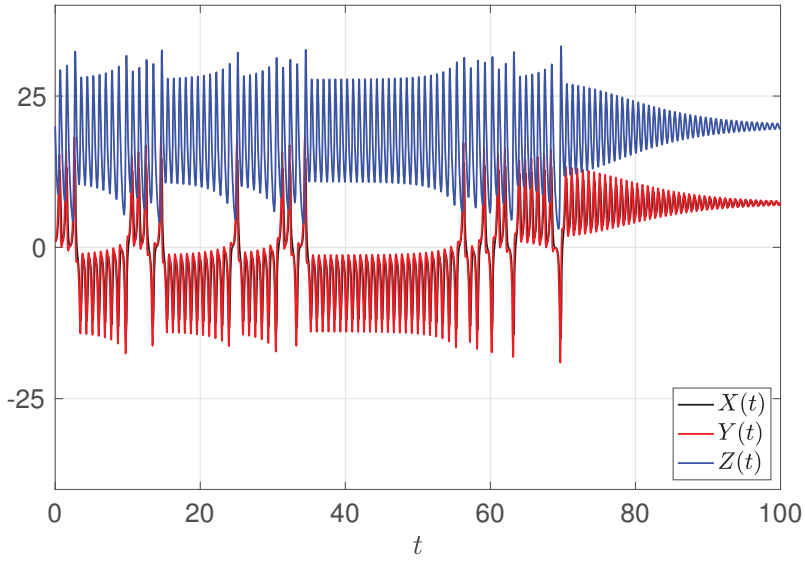

Figure 8: Transient chaos for $r = 20$, $\sigma = 10$ and $b = 8/3$. Note that for $t > 75$ the trajectory is spiraling towards $\boldsymbol{C}^+$ and will eventually get there in an infinite time.

have seen that volumes in the phase space shrinks to zero asymptotically fast in time. Moreover, there exists an ellipsoid that behaves like a trapping region (positively invariant set).

The natural question at this point is: is what is attracting the trajectories entering the ellipsoid for $r > r_H$? Of course it cannot be any of the fixed points since they are all unstable. How about a stable isolated *limit cycle* living within the ellipsoid?

Ruling out stable limit cycles. Lorenz came up with an ingenious heuristic approach to rule out the existence of stable limit cycles within the ellipsoidal trapping region for $r > r_H$. To this end, let us set $\sigma = 10$ and $b = 8/3$. This set of parameters yields $r_H = 24.74$. We choose $r = 28$, which is greater than r_H so that no stable fixed points exist, and plot one trajectory of the system corresponding to and arbitrary initial condition for sufficiently long time. With such trajectory available we can identify the relative maxima of the phase variable $Z(t)$ (see Figure 9) Let us call such sequence of relative maxima

$$\{z_1, z_2, z_3, \ldots\}. \tag{38}$$

Next, look for a map f that takes in one relative maximum and it returns the next one, i.e.,

$$z_{n+1} = f(z_n). \tag{39}$$

The map f is called *Lorenz's map* and it is plotted in Figure 10 using simulation data shown in Figure 9.

Period-1 orbits: A period-1 orbit, i.e. a state in which the previous relative maximum is mapped to itself, is identified by the condition

$$z^* = f(z^*), \tag{40}$$

i.e., it is a fixed point of the Lorenz map (see Figure 10). Of course if such fixed point is stable then $Z(t)$ should eventually hit the basin of attraction of such point and settle to a period-1 orbit. To study stability of z^* we investigate the dynamics of a small perturbation η_0 via the iteration

$$z^* + \eta_{n+1} = f(z^* + \eta_n) \simeq f(z^*) + f'(z^*)\eta_n. \tag{41}$$

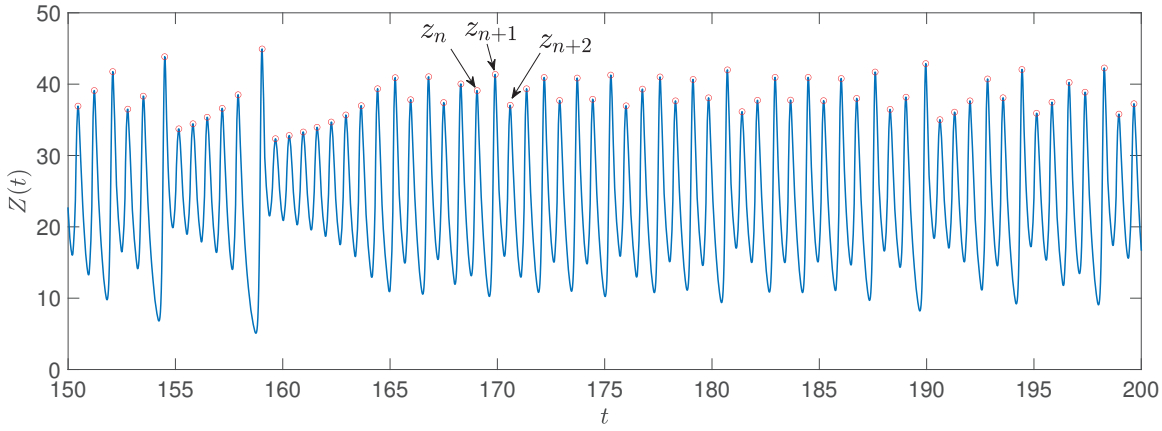

Figure 9: Trajectory of the Lorenz system (8) for $r = 28$, $\sigma = 10$ and $b = 8/3$. Shown is the phase variable $Z(t)$ and its maxima z_n. A necessary condition for the system to settle on a stable periodic orbit is that $Z(t)$ repeats itself after some finite period of time.

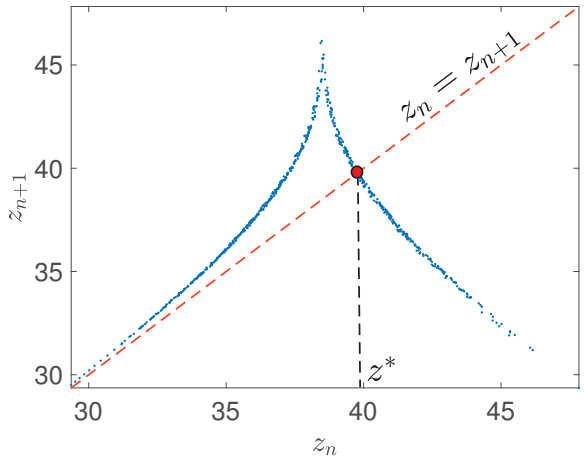

Figure 10: Lorenz's map for $r = 28$, $\sigma = 10$ and $b = 8/3$. Note that blue points are not exactly sitting on a line but rather on an very thin set.

Recalling (40), we see that the perturbation η_n satisfies

$$\eta_{n+1} = f'(z^*)\eta_n. \tag{42}$$

Taking the absolute value and iterating back to the initial perturbation yields

$$|\eta_{n+1}| = \left|f'(z^*)\right| |\eta_n| = \left|f'(z^*)\right|^2 |\eta_{n-1}| = \cdots = \left|f'(z^*)\right|^n |\eta_0| \,. \tag{43}$$

This equation shows that $|\eta_{n+1}| \to 0$ as n goes to infinity if and only if

$$\left|f'(z^*)\right| < 1. \tag{44}$$

However, the numerical results shown in Figure 10, suggest that the Lorenz map satisfies instead

$$|f'(z)| > 1 \qquad \text{for all } z. \tag{45}$$

Hence, period-1 orbits are *unstable*.

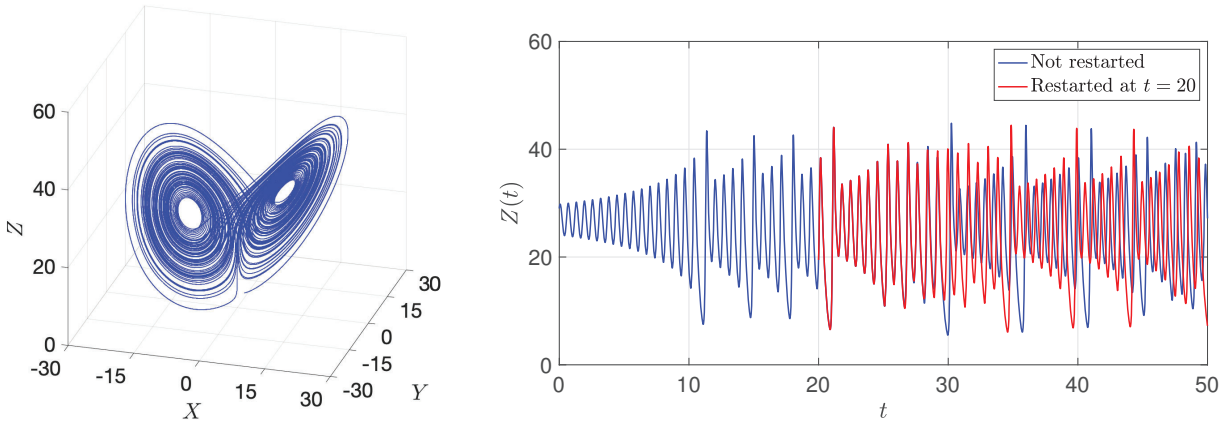

Figure 11: (a)Lorenz's attractor for $r = 28$, $\sigma = 10$ and $b = 8/3$. Shown is one orbit converging to the attractor as t increases. (b) Sensitivity to initial conditions. Integration of the Lorenz system with parameters $r = 28$, $\sigma = 10$ and $b = 8/3$ is restarted at $t = 20$ with an initial condition taken from the non-restarted simulation and rounded to three decimal digits.

Period-2 orbits: By following a similar argument it is possible to rule out stability of period-2 orbits. Such orbits define a cycle satisfying

$$z^* = f(f(z^*)). \tag{46}$$

The stability of period-2 orbits can be studied as before, by investigating how a small perturbation η_0 in a neighborhood of z^* propagates as the Lorenz map is iterated (46). We have,

$$z^* + \eta_{n+1} = f(f(z^* + \eta_n)) = f(f(z^*) + f'(z^*)\eta_n)) = f(f(z^*)) + f'(f'(z^*))f'(z^*)\eta_n, \tag{47}$$

i.e., (using (46))

$$\eta_{n+1} = f'(f'(z^*))f'(z^*)\eta_n \qquad \Rightarrow \qquad |\eta_{n+1}| = \left|f'(f'(z^*))f'(z^*)\right| |\eta_n| \,. \tag{48}$$

Hence a necessary and sufficient condition for stability of period-2 orbits is

$$\left|f'(f'(z^*))f'(z^*)\right| = \left|f'(f'(z^*))\right| \left|f'(z^*)\right| < 1, \tag{49}$$

which is impossible because of (45). Hence there are no stable period-2 orbits.

Period-p orbits: By following a similar argument it is straightforward to show that if (45) is satisfied then there are no stable period-p orbits.

In summary, there is no stable limit cycle within the ellipsoidal trapping region. What is attracting all trajectories then?

The Lorenz attractor. What actually happens to the trajectories of the Lorenz system (8) for $r = 28$ ($\sigma = 10$ and $b = 8/3$) is that they are all attracted by a "non-standard" geometric object (a *strange attractor*) with Hausdorff dimension[4] 2.0627, i.e., not a surface nor a volume but something in-between, i.e., "almost a surface". The "almost" part (and the reason why the Hausdorff dimension is not an integer) is related to the roughness of the surface, which makes it look like a fractal object. The existence of the

[4]The Hausdorff dimension is a measure of dimension that was introduced in 1918 by the mathematician Felix Hausdorff. Hausdorff dimension coincides with regular dimension of smooth objects such as surfaces (dim=2) and volumes (dim=3). The calculation of the Hausdorff dimension is usually done numerically, e.g., in the paper *"The fractal property of the Lorenz attractor"*, Physica D, vol. **190** (2004) 115–128.

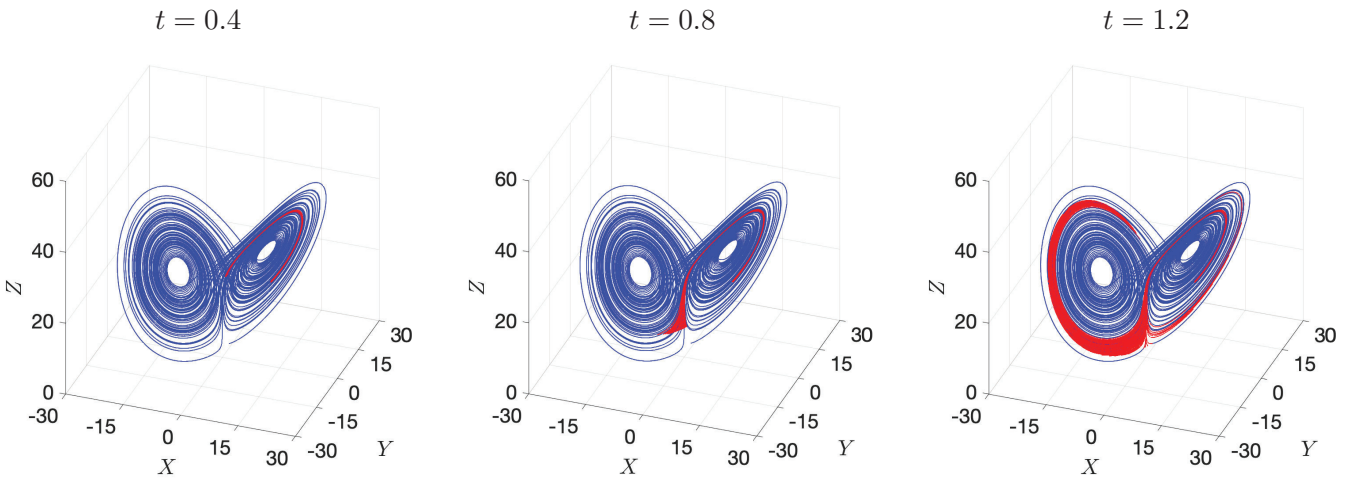

Figure 12: (a)Lorenz's attractor for $r = 28$, $\sigma = 10$ and $b = 8/3$, sensitivity to initial conditions. Shown are trajectories corresponding to a small ball of initial conditions placed nearby the attractor. As time increases such small ball of red initial conditions paints the entire attractor.

strange attractor for the Lorenz system was established in 1999 by Warwick Tucker in his PhD thesis, and in a follow-up paper titled *"The Lorenz attractor exists"* (C. R. Acad. Sci. Paris, vol. **328**, pp. 1197-1202). The proof was based on a combination of normal form theory and rigorous numerical computations. In other words, rather than producing a traditional mathematical proof, Tucker constructed an algorithm which, if successfully executed, proves the existence of the strange attractor.

The Lorenz attractor yields long-term *aperiodic behavior* of all trajectories not sitting on the Z-axis, and a high *sensitivity to initial conditions*. In Figure 12(a) we plot one trajectory of (8) for $r = 28$, $\sigma = 10$ and $b = 8/3$. It is seen that such trajectory settles to an attractor that resemble a butterfly (hence the name "butterfly attractor"). In Figure 12(b) we demonstrate what happens to a trajectory if the integration process is restarted at $t = 20$ with an initial condition taken from the non-restarted simulation and rounded to three decimal digits. The sensitivity to initial condition is also demonstrated in Figure **??**

Appendix A: Liouville's theorem

In this appendix we study how the volume of a compact region $D_0 \subset \mathbb{R}^n$ changes in time when all of its points $\boldsymbol{x}_0 \in D_0$ are advected by the flow generated by the n-dimensional dynamical system

$$\begin{cases} \dfrac{d\boldsymbol{x}}{dt} = \boldsymbol{f}(\boldsymbol{x}), \\ \boldsymbol{x}(0) = \boldsymbol{x}_0. \end{cases} \tag{50}$$

To this end, we assume that $\boldsymbol{f}(\boldsymbol{x})$ is at least continuously differentiable in $\boldsymbol{x}$m and recall that the volume of a region $D(t)$ advected by the flow generated by (50) can be expressed as (see Figure 13)

$$V(t) = \int_{D(t)} 1 d\boldsymbol{x} \tag{51}$$

where $d\boldsymbol{x} = dx_1 \cdots dx_n$. Since the flow $\boldsymbol{X}(t, \boldsymbol{x}_0)$ is invertible, we can transform the coordinates back to $\boldsymbol{x}_0$ and write the integral (51) as

$$V(t) = \int_{D_0} \det\left(\frac{\partial X(t, \boldsymbol{x}_0)}{\partial \boldsymbol{x}_0}\right) d\boldsymbol{x}_0, \tag{52}$$

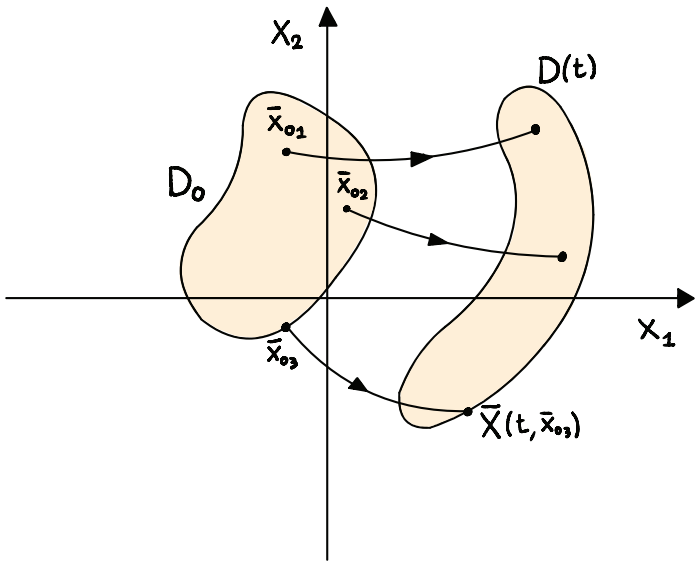

Figure 13: Sketch showing how a domain $D_0 \subset \mathbb{R}^2$ is transported to $D(t) \subset \mathbb{R}^2$ by the flow $\boldsymbol{X}(t,\boldsymbol{x}_0)$ generated by the the dynamical system (50). The rate of change in time of the volume/area of $D(t)$, i.e., $dV(t)/dt$ is given by Liouville's Theorem 2.

where

$$\det\left(\frac{\partial \boldsymbol{X}(t,\boldsymbol{x}_0)}{\partial \boldsymbol{x}_0}\right) = \det\left(\begin{bmatrix} \frac{\partial X_1(t,\boldsymbol{x}_0)}{\partial x_{01}} & \cdots & \frac{\partial X_1(t,\boldsymbol{x}_0)}{\partial x_{0n}} \\ \vdots & \ddots & \vdots \\ \frac{\partial X_n(t,\boldsymbol{x}_0)}{\partial x_{01}} & \cdots & \frac{\partial X_n(t,\boldsymbol{x}_0)}{\partial x_{0n}} \end{bmatrix}\right) \tag{53}$$

is the Jacobian determinant of the coordinate change[5] $\boldsymbol{X}(t,\boldsymbol{x}_0) \leftrightarrow \boldsymbol{x}_0$ at each time t.

Theorem 1. Let $\boldsymbol{X}(t,\boldsymbol{x}_0)$ be the flow generated by (50). Then the Jacobian determinant of $\boldsymbol{X}(t,\boldsymbol{x}_0)$, i.e., (53), satisfies

$$\frac{\partial}{\partial t}\det\left(\frac{\partial \boldsymbol{X}(t,\boldsymbol{x}_0)}{\partial \boldsymbol{x}_0}\right) = \nabla\cdot\boldsymbol{f}(\boldsymbol{X}(t,\boldsymbol{x}_0))\det\left(\frac{\partial \boldsymbol{X}(t,\boldsymbol{x}_0)}{\partial \boldsymbol{x}_0}\right). \tag{54}$$

Proof. Let us prove the theorem for two-dimensional dynamical systems. In this case, the determinant (53) can be written as

$$\det\left(\frac{\partial \boldsymbol{X}(t,\boldsymbol{x}_0)}{\partial \boldsymbol{x}_0}\right) = \frac{\partial X_1}{\partial x_{01}}\frac{\partial X_2}{\partial x_{02}} - \frac{\partial X_2}{\partial x_{01}}\frac{\partial X_1}{\partial x_{02}}. \tag{55}$$

Differentiate (55) with respect to time to t to obtain

$$\begin{aligned}\frac{\partial}{\partial t}\det\left(\frac{\partial \boldsymbol{X}(t,\boldsymbol{x}_0)}{\partial \boldsymbol{x}_0}\right) =& \frac{\partial}{\partial x_{10}}\left(\frac{dX_1(t,\boldsymbol{x}_0)}{dt}\right)\frac{\partial X_2(t,\boldsymbol{x}_0)}{\partial x_{20}} + \frac{\partial X_1(t,\boldsymbol{x}_0)}{\partial x_{10}}\frac{\partial}{\partial x_{20}}\left(\frac{dX_2(t,\boldsymbol{x}_0)}{dt}\right) - \\ & \frac{\partial}{\partial x_{20}}\left(\frac{dX_1(t,\boldsymbol{x}_0)}{dt}\right)\frac{\partial X_2(t,\boldsymbol{x}_0)}{\partial x_{10}} - \frac{\partial X_1(t,\boldsymbol{x}_0)}{\partial x_{20}}\frac{\partial}{\partial x_{10}}\left(\frac{dX_2(t,\boldsymbol{x}_0)}{dt}\right).\end{aligned} \tag{56}$$

At this point we recall that

$$\frac{dX_i(t,\boldsymbol{x}_0)}{dt} = f_i\left(X_1(t,\boldsymbol{x}_0), X_2(t,\boldsymbol{x}_0)\right), \qquad i=1,2, \tag{57}$$

[5] We know that the flow map $\boldsymbol{X}(t,\boldsymbol{x}_0)$ generated by a smooth (at least C^1) dynamical system is invertible at each point where the solution to (50) exists and is unique (see the course note 3).

which implies that

$$\begin{aligned}
\frac{\partial}{\partial x_{10}}\left(\frac{dX_1(t,\boldsymbol{x}_0)}{dt}\right) &= \frac{\partial f_1\left(X_1(t,\boldsymbol{x}_0),X_2(t,\boldsymbol{x}_0)\right)}{\partial x_{10}} = \frac{\partial f_1}{\partial x_1}\frac{\partial X_1}{\partial x_{10}} + \frac{\partial f_1}{\partial x_2}\frac{\partial X_2}{\partial x_{10}},\\
\frac{\partial}{\partial x_{20}}\left(\frac{dX_1(t,\boldsymbol{x}_0)}{dt}\right) &= \frac{\partial f_1\left(X_1(t,\boldsymbol{x}_0),X_2(t,\boldsymbol{x}_0)\right)}{\partial x_{20}} = \frac{\partial f_1}{\partial x_1}\frac{\partial X_1}{\partial x_{20}} + \frac{\partial f_1}{\partial x_2}\frac{\partial X_2}{\partial x_{20}},\\
\frac{\partial}{\partial x_{10}}\left(\frac{dX_2(t,\boldsymbol{x}_0)}{dt}\right) &= \frac{\partial f_2\left(X_1(t,\boldsymbol{x}_0),X_2(t,\boldsymbol{x}_0)\right)}{\partial x_{10}} = \frac{\partial f_2}{\partial x_1}\frac{\partial X_1}{\partial x_{10}} + \frac{\partial f_2}{\partial x_2}\frac{\partial X_2}{\partial x_{10}},\\
\frac{\partial}{\partial x_{20}}\left(\frac{dX_2(t,\boldsymbol{x}_0)}{dt}\right) &= \frac{\partial f_2\left(X_1(t,\boldsymbol{x}_0),X_2(t,\boldsymbol{x}_0)\right)}{\partial x_{20}} = \frac{\partial f_2}{\partial x_1}\frac{\partial X_1}{\partial x_{20}} + \frac{\partial f_2}{\partial x_2}\frac{\partial X_2}{\partial x_{20}}.
\end{aligned}$$

A substitution of these expressions back into (56) yields

$$\begin{aligned}
\frac{\partial}{\partial t}\det\left(\frac{\partial \boldsymbol{X}(t,\boldsymbol{x}_0)}{\partial \boldsymbol{x}_0}\right) =& \frac{\partial f_1}{\partial x_1}\frac{\partial X_1}{\partial x_{10}}\frac{\partial X_2}{\partial x_{20}} + \frac{\partial f_1}{\partial x_2}\frac{\partial X_2}{\partial x_{10}}\frac{\partial X_2}{\partial x_{20}} + \frac{\partial f_2}{\partial x_1}\frac{\partial X_1}{\partial x_{20}}\frac{\partial X_1}{\partial x_{10}} + \frac{\partial f_2}{\partial x_2}\frac{\partial X_2}{\partial x_{20}}\frac{\partial X_1}{\partial x_{10}} -\\
& \frac{\partial f_1}{\partial x_1}\frac{\partial X_1}{\partial x_{20}}\frac{\partial X_2}{\partial x_{10}} - \frac{\partial f_1}{\partial x_2}\frac{\partial X_2}{\partial x_{20}}\frac{\partial X_2}{\partial x_{10}} - \frac{\partial f_2}{\partial x_1}\frac{\partial X_1}{\partial x_{10}}\frac{\partial X_1}{\partial x_{20}} - \frac{\partial f_2}{\partial x_2}\frac{\partial X_2}{\partial x_{10}}\frac{\partial X_1}{\partial x_{20}},\\
=& \underbrace{\left(\frac{\partial f_1}{\partial x_1} + \frac{\partial f_2}{\partial x_2}\right)}_{\nabla\cdot\boldsymbol{f}}\det\left(\frac{\partial \boldsymbol{X}(t,\boldsymbol{x}_0)}{\partial \boldsymbol{x}_0}\right),
\end{aligned}$$

which proves the theorem. A similar proof can be given in n dimensions using the expression of the determinant of a $n\times n$ matrix in terms of the Levi-Civita symbol.

□

Note that at $t=0$ we have $\boldsymbol{X}(0,\boldsymbol{x}_0)=\boldsymbol{x}_0$ and therefore

$$\det\left(\frac{\partial \boldsymbol{X}(0,\boldsymbol{x}_0)}{\partial \boldsymbol{x}_0}\right) = \det(\boldsymbol{I}) = 1. \tag{58}$$

With this initial condition it is immediate to integrate the (separable) ODE (54) to obtain

$$\det\left(\frac{\partial \boldsymbol{X}(t,\boldsymbol{x}_0)}{\partial \boldsymbol{x}_0}\right) = \exp\left[\int_0^t \nabla\cdot\boldsymbol{f}(\boldsymbol{X}(\tau,\boldsymbol{x}_0))d\tau\right] \tag{59}$$

We now have all element to prove the following theorem due to Liouville.

Theorem 2 (Liouville's theorem)**.** The volume $V(t)$ of a compact region $D(t)\subset\mathbb{R}^n$ advected by the flow $\boldsymbol{X}(t,\boldsymbol{x}_0)$ generated by a smooth dynamical system of the form (50) satisfies

$$\frac{dV(t)}{dt} = \int_{D(t)} \nabla\cdot\boldsymbol{f}(\boldsymbol{x})d\boldsymbol{x} \tag{60}$$

Proof. The volume of $D(t)$ can be expressed as (see equation (52))

$$V(t) = \int_{D_0} \det\left(\frac{\partial X(t,\boldsymbol{x}_0)}{\partial \boldsymbol{x}_0}\right) d\boldsymbol{x}_0 \tag{61}$$

Differentiating with respect to time and using (54) yields

$$\begin{aligned}\frac{dV(t)}{dt} =& \frac{\partial}{\partial t}\int_{D_0} \det\left(\frac{\partial X(t,\boldsymbol{x}_0)}{\partial \boldsymbol{x}_0}\right) d\boldsymbol{x}_0 \\ =& \int_{D_0} \frac{\partial}{\partial t} \det\left(\frac{\partial X(t,\boldsymbol{x}_0)}{\partial \boldsymbol{x}_0}\right) d\boldsymbol{x}_0 \\ =& \int_{D_0} \nabla\cdot\boldsymbol{f}\left(\boldsymbol{X}(t,\boldsymbol{x}_0)\right) \det\left(\frac{\partial X(t,\boldsymbol{x}_0)}{\partial \boldsymbol{x}_0}\right) d\boldsymbol{x}_0 \\ =& \int_{D(t)} \nabla\cdot\boldsymbol{f}\left(\boldsymbol{x}\right) d\boldsymbol{x}. \end{aligned} \tag{62}$$

□